DEVELOPMENT OF EYE-SAFE LASER RANGE FINDER

Capt. Sahapong Kruapech RTN

A Thesis Submitted in Partial Fulfillment of the Requirements for the Degree of Doctor of Philosophy in Laser Technology

Suranaree University of Technology

Academic Year 2009

การพัฒนาอุปกรณ์หาพิสัยด้วยเลเซอร์ชนิดปลอดภัยต่อตา

น.อ. สหพงษ์ เครือเพ็ชร ร.น.

วิทยานิพนธ์นี้เป็นส่วนหนึ่งของการศึกษาตามหลักสูตรปริญญาวิทยาศาสตรดุษฎีบัณฑิต
สาขาวิชาเลเซอร์เทคโนโลยี
มหาวิทยาลัยเทคโนโลยีสุรนารี
ปีการศึกษา 2552

DEVELOPMENT OF EYE-SAFE LASER RANGE FINDER

Suranaree University of Technology has approved this thesis submitted in partial fulfillment of the requirements for the Degree of Doctor of Philosophy.

Thesis Examining Committee

_____
(Asst. Prof. Dr. Chinorat Kobdaj)
Chairperson

_____
(Prof. Dr. Joewono Widjaja)
Member (Thesis Advisor)

_____
(Assoc. Prof. Dr. Bancha Panacharoensawad)
Member

_____
(Prof. Dr. Yupeng Yan)
Member

_____
(Asst. Prof. Dr. Eckart Schulz)
Member

_____	_____
(Prof. Dr. Pairote Sattayatham)	(Assoc. Prof. Dr. Prapun Manyum)
Vice Rector for Academic Affairs	Dean of Institute of Science

สหพงษ์ เครือเพ็ชร : การพัฒนาอุปกรณ์หาพิสัยด้วยเลเซอร์ชนิดปลอดภัยต่อตา (DEVELOPMENT OF LASER RANGE FINDER) อาจารย์ที่ปรึกษา : ศาสตราจารย์ ดร. ยูโวโน วิดจายา, 79 หน้า

ในงานวิทยานิพนธ์นี้ ได้ทำการศึกษากล้องวัดระยะทางด้วยแสงเลเซอร์ชนิดปลอดภัยต่อตาที่ใช้แท่งเลเซอร์ Er:Glass และปั๊มพลังงานด้วยเลเซอร์ไดโอด กล้องวัดระยะทางนี้แตกต่างจากกล้องวัดระยะทางทั่วไปและมีข้อดีกว่าหลายประการดังต่อไปนี้ (1) ปลอดภัยต่อตา เนื่องจากเลเซอร์ให้แสงความยาวคลื่น 1540 nm ซึ่งเป็นย่านที่ถูกดูดกลืนได้ดีด้วยกระจกตา ทำให้แสงไม่สามารถผ่านไปถึงจอรับภาพได้ (2) เลเซอร์ไดโอดที่ใช้ปั๊มพลังงานมีขนาดเล็กกระทัดรัด น้ำหนักเบาและทำงานด้วยวงจรที่ไม่ซับซ้อนและ (3) ภายในหัวเลเซอร์ได้ติดตั้งโฟโตไดโอด เพื่อรับแสงที่ออกจากทางด้านหลังของแท่งเลเซอร์ ทำให้ได้สัญญาณเริ่มต้น ในรูปสัญญาณอิเล็กทรอนิกส์และแยกต่างหากจากสัญญาณที่สะท้อนกลับจากเป้า ดังนั้น กล้องวัดระยะทางใหม่นี้จึงมีระบบทัศนศาสตร์และอิเล็กทรอนิกส์ที่ไม่ซับซ้อน

นอกจากระบบใหม่ที่นำเสนอแล้ว ยังได้พัฒนาสมการระยะทางทฤษฎีใหม่สำหรับการวัดระยะทางด้วยแสงเลเซอร์ที่ใช้ลำแสง Gaussian ซึ่งยังไม่มีการนำเสนอมาก่อน สมการระยะทางใหม่นี้มีข้อดีกว่าสมการระยะทางทั่วไปคือ สามารถประยุกต์ใช้อย่างอิสระกับเป้าขนาดใดก็ได้และระยะทางเท่าไรก็ได้ ขณะเดียวกันเราได้นำเสนอสัมประสิทธิ์ปฏิบัติการใหม่ที่สามารถนำมาใช้คำนวณพลังงานแสงเลเซอร์ที่สะท้อนกลับจากเป้าอย่างถูกต้อง เพื่อนำไปคำนวณระยะทางไกลสุดของระบบวัดระยะทางด้วยแสงเลเซอร์

สาขาวิชาเทคโนโลยีเลเซอร์และโฟตอนนิกส์ ลายมือชื่อนักศึกษา_____

ปีการศึกษา 2552 ลายมือชื่ออาจารย์ที่ปรึกษา_____

ลายมือชื่ออาจารย์ที่ปรึกษาร่วม_____

SAHAPONG KRUAPECH : DEVELOPMENT OF EYE-SAFE LASER RANGE FINDER. THESIS ADVISOR : PROF. JOEWONO WIDJAJA, Ph.D. 79 PP.

LASER RANGE FINDER/ EYE-SAFE LASER/ GAUSSIAN BEAM RANGE EQUATION

A new handheld eye-safe laser range finder using a laser diode pumped Er: Glass is studied. In contrast to conventional laser range finder using a flash-lamp pumped solid-state laser, the new laser range finding system excels in the following: (1) eye safe, because the laser emits light at 1540 nm which is strongly absorbed by the cornea and cannot reach the retina; (2) the pumping laser diode is compact, light weight and does not require complex driving circuit; and (3) a photodiode is installed in the laser head to detect light from the back end of a lasing rod. This produces a start signal which is already in electronic form and is separated from the echo signal. Thus, it simplifies both optics and electronics of the new laser range finder.

Besides the new proposed system, we also develop a new theoretical range equation for laser rangefinder based on Gaussian beam analysis, which has never been reported before. The Gaussian beam range equation has an advantage over the conventional range equations in that it can be applied independently to any size and range of target. We also propose and define a new operational coefficient which can be used for correctly estimating the returned light power and hence the maximum detectable range of a laser range finder.

School of Laser Technology and Photonics
Academic Year 2009

Student's Signature _____
Advisor's Signature_____
Co-advisor's Signature _____

ACKNOWLEDGEMENTS

This thesis would not have been completed without assistance and guidance by many persons in various ways. It is my pleasure to express my gratitude to the following persons for their contribution.

Firstly, I would like to thank Prof. Dr. Joewono Widjaja, my thesis advisor, for the invaluable advice, encouraging and the unfailing support during the course of my studies at the School of Laser Technology and Photonics.

I also want to thank Prof. Dr. Suganda Jutamulia for his enlightening guidance and encouragement. His bright ideas have been of vital importance for this thesis.

I express my appreciation to Asst. Prof. Kanokpoj Areekul and Assoc. Prof. Dr. Bancha Panacharoensawad, Physics Department, Kasetsart University for their valuable collaboration and inspiring discussion.

Finally, I would like to thank my wife Manusawee and my daughter Sydney for their love and patience during these years.

Sahapong Kruapech

CONTENTS

Page

CONTENTS (Continued)

Page

CONTENTS (Continued)

Page

LIST OF TABLES

Table **Page**

LIST OF FIGURES

LIST OF FIGURES (Continued)

LIST OF FIGURES (Continued)

LIST OF FIGURES (Continued)

Figure **Page**

CHAPTER I

INTRODUCTION

1.1 General Background

Laser range finder (LRF) is an instrument that measures distance by measuring the time necessary for electromagnetic radiation to travel to target of interest and back to a receiver at a speed equal to c/n where n is the optical refractive index of a medium and c is the speed of light in vacuum. It operates on the same basic principles as microwave radar except it transmits light whose wavelength is much shorter than microwave. Because it operates at much shorter wavelengths, it is capable of measuring distance with higher accuracy and resolution.

LRF was one of the first and successful applications of laser technology so far (Stitch, 1972). In military applications, range finding systems are needed to compute trajectory of cannons or missiles in order to accurately destroy enemy target. Today LRFs are considered a necessary tool in all modern fire control systems in all sophisticated armies. We find them in artillery, infantry and armored vehicles as well as in navy (both costal artillery and ship borne) and air forces (anti aircraft as well as airborne).

In this research, we select LRF using pulsed time-of-flight (TOF) technique, because it has advantages over other techniques and is suitable for military applications as follow (Forrester and Hulme, 1981).

- The returned signal follows essentially the same path to a receiver located coaxially with or in the close proximity to the transmitter. We can build a system with small size, light weight and portable.
- The absolute range to the observed target is directly available as an output with no complicated analysis required, and the technique is not based on any assumptions concerning the planar properties or orientation of the target surface.
- Range accuracy is maintained in a linear fashion as long as reliable echo detection is sustained, while the other techniques suffer diminishing accuracy as distance to the target increase.

For military usage, handheld range finders have been proven to be among the most important equipment in battle fields. Currently, there are about 550 units of four different models of handheld LRF deployed in the Thai military. These LRFs were purchased from foreign manufacturers more than a decade ago. Because of getting old and wearing out, the Thai military has to stock four different sets of laser range finder spare parts which are expensive and hard to find. This causes disadvantages in terms of logistic and maintenance. Furthermore, these LRFs are not operated with eye-safe laser sources. Thus without safety precautions, our military personnel are exposed to danger of blindness when they operate the laser range finder in practice or real battle field or even in the repair process. For these reasons, it is important to replace non eye-safe LRFs in the Thai military with eye-safe ones.

1.2 Overview of Laser Range Finder

There are many methods to measure distance using laser light, which are based on: (1) interferometry, (2) beam modulation telemetry, and (3) time of flight (Amann *et al.*, 2001). They provide different ranges and accuracies. The first method is based on an interferometry in which the frequency of a cw laser itself is used. With this fringe counting technique, displacement in distance can be measured in the order of wavelength of the used laser light. This technique is generally used for relative displacement measurements in laboratory environment. The second one utilizes an amplitude modulated cw laser. In this method, the laser beam is directed at a target. When the light signal is reflected back its phase is shifted proportionally by the range being measured. Since the phase measurement is unambiguous only up to the range corresponding to 2π radians, a method of removing range ambiguities using several frequencies must be used. This technique has an accuracy of a few millimeter orders at ranges of several kilometers. In the third method, a narrow pulse (usually less than 50 ns) is transmitted to the target. Its time of flight which is proportional to the range is measured.

The time of flight method is the most representative principle of LRFs (Stitch, 1972). This method has definitely moved from laboratory to field use and developed into full production. For this reason, this research work will deal with only this type of LRF. The principle of time-of-flight LRF is similar to the principle of radar. Instead of using radio waves, the range finder uses light waves. Both techniques are based on the transmission of a short pulse of electromagnetic radiation and the reception of back scattered signals from a target. The time between the transmission and reception

of the pulse or time of flight t is measured and the distance d is calculated on the basis of the relationship $d = ct/2$, where c is the velocity of light.

A typical time-of-flight LRF contains a laser transmitter, a receiver channel, and a range converter unit as shown in Fig. 1.1. The light pulse is sent by the laser transmitter to the target through a collimator. The transmitter consists of a laser head which is usually a Q-switched solid state laser such as Nd:YAG (Corcoran, 1991), (Wu *et al*., 2004) or laser diode (Perger *et al*., 1991), and a collimator. The receiver channel consists of a lens, a photodiode, a transimpedance type preamplifier, a voltage type post amplifier and a timing discriminator. The timing discriminator converts the measured analog pulses into logic level pulses.

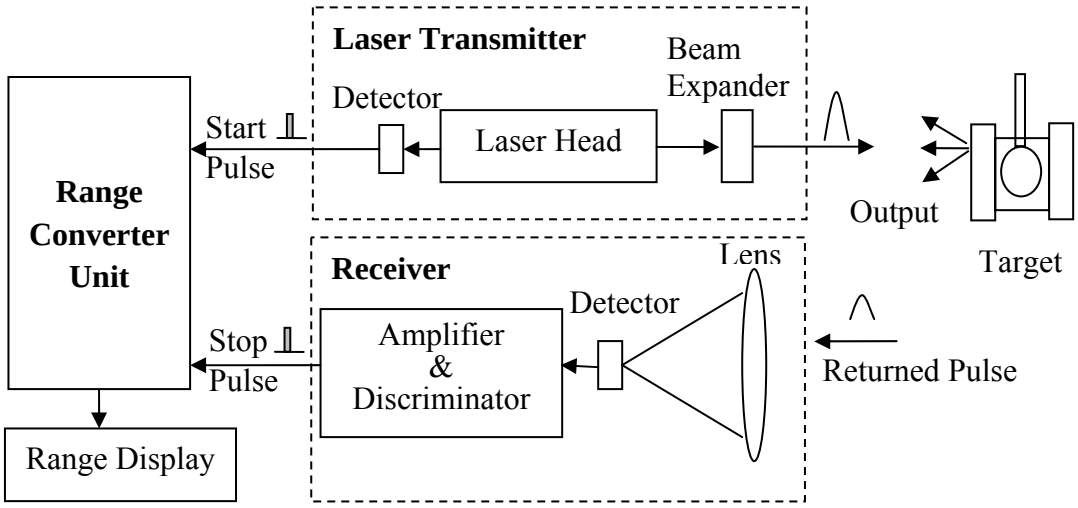

Figure 1.1 Block diagram of a time-of-flight laser range finder.

Figure 1.2 shows a leading edge timing discriminator technique which is used for pulse converter (Wagner *et al.*, 2004). When a leading edge of an analog input signal reaches a certain threshold level, a timing discriminator circuit generates a logic pulse. The resultant logic pulses are then fed to a range converter unit, which in

turn gives measurement results in digital form. The most important property of the timing discriminator is to keep the timing moment at the same point of the input pulse at all input amplitudes. The range converter unit measures the total time period counting the digital pulses of an oscillator. The measured range is displayed on the range display such as four-digit LED.

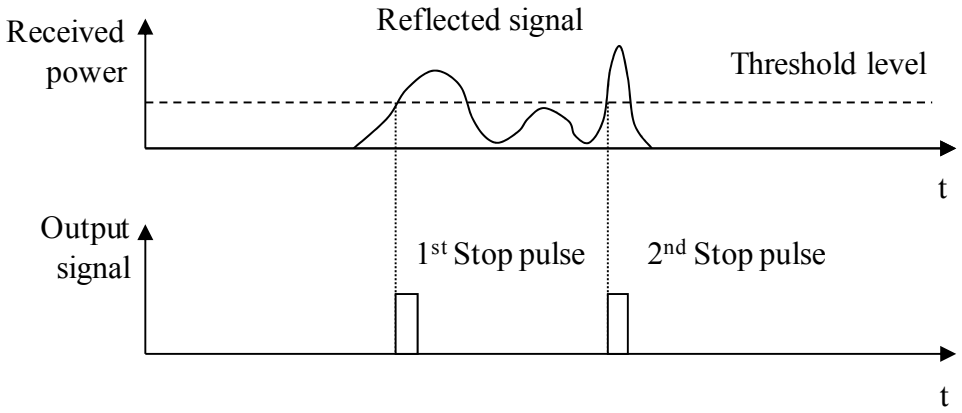

Figure 1.2 Leading edge timing discriminator technique.

The performance of the electronics must be good, because a change of 15 cm in the distance is equivalent to 1 ns change in time, if the measurement is carried out in air. Measuring short time intervals accurately and repeatedly requires wide bandwidth and low noise electronics, because the precision of the instrument is directly related to the slew rate of the measurement pulse and inversely related to the noise level. Other parameters describing the performance of LRF are linearity, stability and walk error. The linearity of the whole device mainly depends on the linearity of the time interval measurement, which can be made good enough by utilizing quartz controlled digital counter. The stability can be improved by using the same path for both start and stop pulses. The walk error means changes in a distance

measurement result as a function of amplitude of the measurement pulse and it is mainly caused by a limited gain bandwidth product of the comparator in the time discriminator (Gedcke, 1968). The walk error can be reduced by using measurement pulses with a high slew rate. It means that laser pulse must be short and powerful and the receiver channel must have sufficiently high bandwidth.

1.3 Significance of the Study

In order to develop and eventually produce LRFs in Thailand, we must first do the research, which must also be suited to Thai situation and condition. The success of the research will include factors of academic originally, military applicability, and manufacturing practicality. To save the country's spending budget and to reduce dependence on other countries, the research on LRF and especially eye-safe LRF is needed. The study reported in this dissertation is the first step of the research and development of eye-safe LRF in Thailand.

In this dissertation, an eye-safe LRF is studied (Franks, 1991). Instead of a flash-lamp pumped laser, an Erbium: Glass diode pumped solid-state laser is used as a light source in the transmitter of the system. Besides transmitting light at the eye-safe wavelength, this laser has several advantages over conventional flash-lamp pumped light sources in that the efficiency is higher and its life time is longer (10^7 shots instead of 10^5 shots); its power supply circuit is easy to handle, because no huge storage capacitor, no high voltage and no triggering transformer are needed. Since its dimension is small and its weight is light, this laser is a good candidate as the light source of a handheld LRF. In the receiver, a PIN photodiode is used, instead of Avalanche photodiode (APD). Although an APD has internal gain and better

responsivity, it needs high bias voltage of 300-500V which is inconvenient and has additional access noise which limits its sensitivity.

We have developed and tested a handheld eye-safe LRF. The constructed system has potential advantages mentioned above including eye-safe, light weight, and cost effective. With further improvements, we expect to be able to detect the returned signal from a target located larger than 2. In addition to the construction and test of the LRF, we have also developed a new theoretical range equation for LRF that has never been reported before. We have also proposed a new operational coefficient to bridge the theoretical high performance and the actual low performance. The new operational coefficient can be used to calibrate the theoretical values to the measured values, and can also be used as a quality indicator of a LRF.

1.4 Organization

This dissertation is organized as follows: Fundamentals of laser range finder as well as optical and electronic systems are presented in Chapter II. Chapter III discusses a novel range equation based on Gaussian shape of laser beam and an operational coefficient for estimation of maximum detectable range. Development of the proposed handheld eye-safe laser range finder and its experimental verifications are discussed in Chapter IV. Conclusions of the dissertation are presented in Chapter V.

CHAPTER II

FUNDAMENTALS OF EYE-SAFE LASER RANGE FINDER

2.1 Need of Range Finder

In a battle field, it is important to know the distance between an enemy target and an artillery launcher in order to have a correct projectile trajectory for destroying the target. Fig. 2.1(a) illustrates a projectile which is fired by aiming a target tank along a line of sight. Since the distance between the launcher and the target is relatively large, and the initial speed of the projectile is limited, the projectile misses the target. Owing to the acceleration of gravity, the projectile will fall to the ground

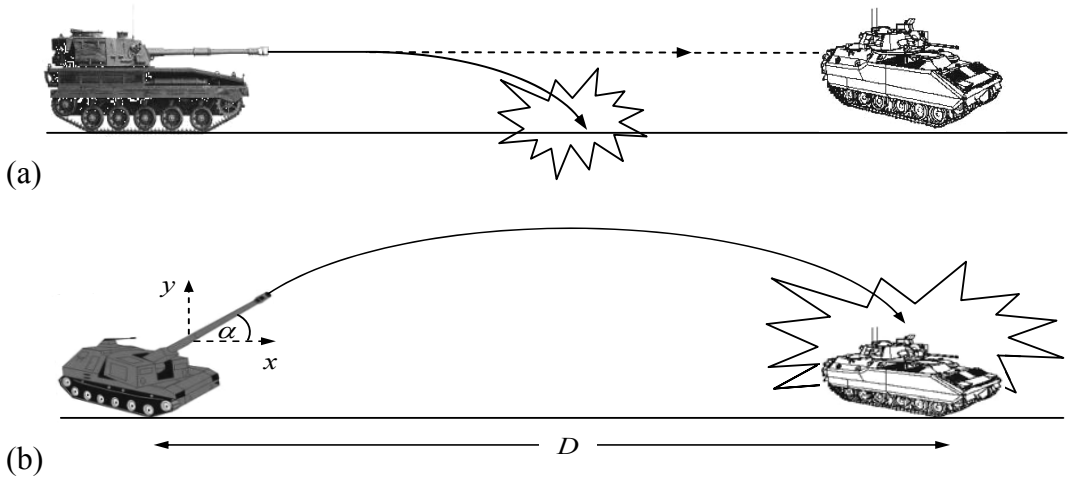

Figure 2.1 Projectile trajectories which are fired (a) along the line of sight and (b) with the angle of inclination to hit the target.

before it hits the target. To balance the effect of gravity, the artillery is fired with an angle of inclination α as shown in Fig. 2.1(b). The angle of inclination depends on the projectile initial speed and the distance between the artillery and the target.

The angle of inclination can be calculated by solving the motion equation into two orthogonal components: the x (horizontal) and the y (vertical) directions. In the x-direction, we have

$$D = vt\cos\alpha, \tag{2.1}$$

and in the y-direction is

$$0 = vt\sin\alpha - \frac{1}{2}gt^2, \tag{2.2}$$

where D is the distance between the artillery launcher and the target, t is the time for projectile to travel to the target, α is the inclination angle of projectile, v is the initial speed of the projectile, and g is the acceleration of gravity. Since t in Eqs. (2.1) and (2.2) must be the same, by combining Eqs. (2.1) and (2.2), we can get the angle of inclination:

$$\alpha = \tan^{-1}\left(\frac{v^2 \pm \sqrt{v^4 - g^2D^2}}{gD}\right). \tag{2.3}$$

Since the acceleration gravity is 9.8 m/s^2 and the initial speed of the projectile is known (e.g., provided by the artillery maker), the distance between the launcher and the target must be sought in order to obtain the correct inclination angle. As a result, the target can be accurately struck.

Although traditional projectile firing is taken as example, the distance between an operator and a target can also be used to calculate a position of the target in GPS (Global Positioning System), where the position of the operator is taken as a reference,

as shown in Fig. 2.2. The position of the target can be further used for firing a missile using advanced navigation devices.

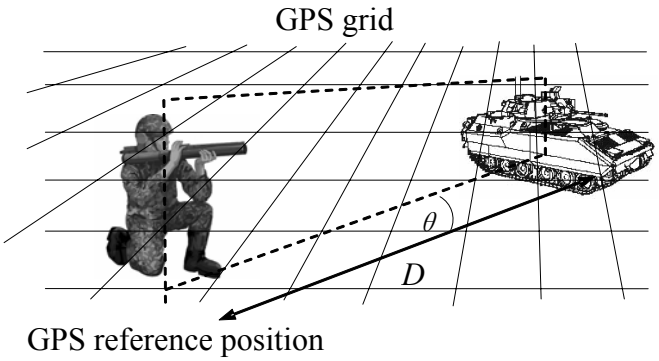

Figure 2.2 The GPS position of the target can be determined using the angle of line of sight θ in the GPS grid and the distance D referring to the GPS position of the operator.

2.2 Distance Measurement

In many cases of distance measurement, we cannot receive cooperation from targets. For example, in a battle field, the target is our enemy. Preferably, the enemy is not even aware that we are measuring its location. There are some optical methods that can accomplish this task. Among them are optical triangulation method and time-of-flight method. The principles of the triangulation and the time-of-flight methods are shown in Figs. 2.3 and 2.4 respectively.

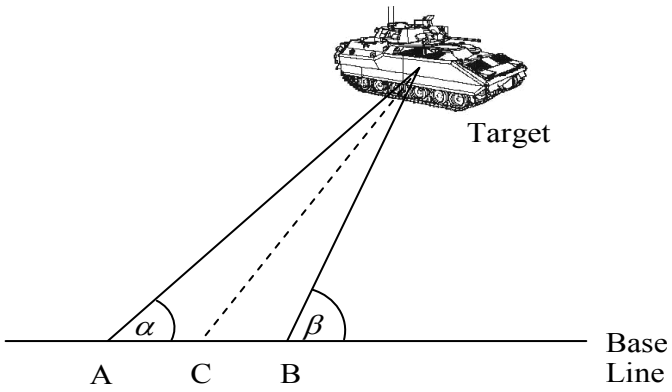

Figure 2.3 Principle of optical triangulation method.

2.2.1 Optical Triangulation Method

In optical triangulation method (Strand, 1983), there are two reference points A and B, which are connected by a base line. The angles of line of sight from A to the target and from B to the target with reference to a base line are α and β, respectively, which can be obtained from observation. Therefore, the triangle with vertex of A, B, and the target can be drawn on a paper. Since the distance between the references A and B is known, the distance between A and the target, or B and the target, can be calculated. In addition, the distance between the target and another point, for example point C, which is the center between A and B, can also be calculated. The accuracy of the distance measurement based on this method depends on the distance of A and B or the length of the base line. If the length of the base line is large, the accuracy is better. Accordingly, this method is not suitable for a handheld device since the separation of A and B is very small compared to the distance to the target.

2.2.2 Time of Flight Method

As shown in Fig. 2.4, the principle of the time-of-flight method is indeed very simple. A light pulse is transmitted toward a target. When the target reflects the light, a portion of the reflected light is detected at the position of a transmitter. Since the speed of light is known, the distance between the target and the transmitter can be calculated from the round trip traveling time of the light pulse. If the light pulse is transmitted at time t_0, and the reflected pulse is detected at time t_D, the distance between the target and the transmitter is

$$R = \frac{(t_D - t_0)c}{2}, \tag{2.4}$$

where c is the speed of light, which is 3×10^8 m/s. In one second, a light pulse travels 300,000 . In other words, the light pulse travels 3 in 10 μs. For example, to have a resolution of 1.5 m, the system must be able to differentiate two pulses reflected by two reflecting surfaces 1.5 m apart. The two pulses are separated by 10 ns.

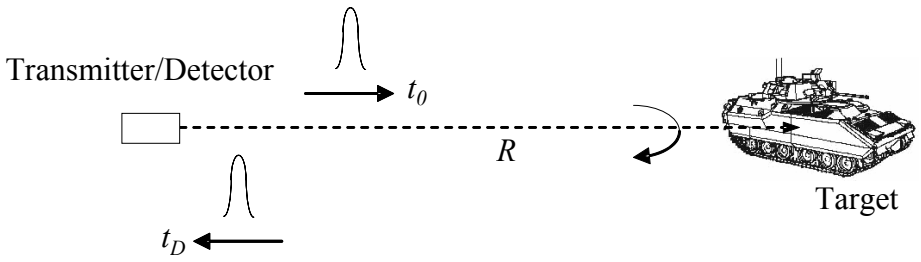

Figure 2.4 Principle of time of flight method.

2.3 Laser Range Finder

If the transmitter is a kind of point source, and the power is spread in a forward hemisphere, the power arriving at a unit area on the hemisphere is given by

$$P_{Hemisphere} = \frac{P_{Transmitter}}{2\pi R^2}, \tag{2.5}$$

where $P_{Transmitter}$ is the power at the transmitter, and R is the radius of the hemisphere. The denominator corresponds to the area of a hemisphere (half of a sphere).

The power arriving at the target is given by

$$P_{Target} = A_{Target} \times \frac{P_{Transmitter}}{2\pi R^2}, \tag{2.6}$$

where A_{Target} is the area of the target and R is the distance between the transmitter and the target. R does not only stand for radius but can also stand for range. From now on, we will refer to the distance between the target and transmitter/detector as “range” or R, and the device for measuring the distance is called “range finder”.

The power of the reflected light, which is detected by the detector will be

$$P_{Detector} = A_{Detector} \times \frac{P_{Target}}{2\pi R^2}. \tag{2.7}$$

where $A_{Detector}$ is the area of the detector. Substituting Eq. (2.6) into Eq. (2.7) yields

$$P_{Detector} = \frac{B}{\left(2\pi R^2\right)^2} \times P_{Transmitter}, \tag{2.8}$$

where B is an arbitrary constant proportional to the product of the target area and the detector area. It is apparent that the detected power is inversely proportional to R^4 of the transmitted power. The transmitter, which is combined with the detector, and the target are illustrated in Fig. 2.5.

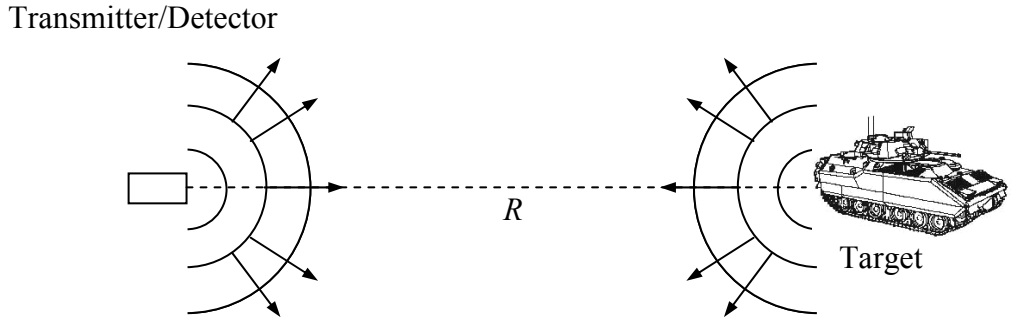

Figure 2.5 The power arriving at the target is inversely proportional to R^2 of the transmitted power, and the power arriving at the detector is inversely proportional to the R^4 of the transmitted power.

It is of course difficult to detect the reflected light, since its power is attenuated by $1/R^4$ when it arrives at the detector. R is very large, at least 1 . The range finder could not be possibly built until the invention of laser. Accordingly, a range finder using a laser is called a "laser range finder" or LRF.

A laser can emit a high power light. Furthermore, in contrast to a point light source, light emitted by a laser is ideally collimated, meaning that the light is not spread in hemisphere. Ideally, the light pulse travels to the target in a straight line without spreading as illustrated in Fig. 2.6. Therefore, the power arriving at the target is the same as the power transmitted by the transmitter. The power arriving at the detector is thus inversely proportional to R^2 instead of R^4 of the transmitted power.

$$P_{Detector} = \frac{B'}{2\pi R^2} \times P_{Transmitter} \ , \tag{2.11}$$

where B' is another arbitrary constant.

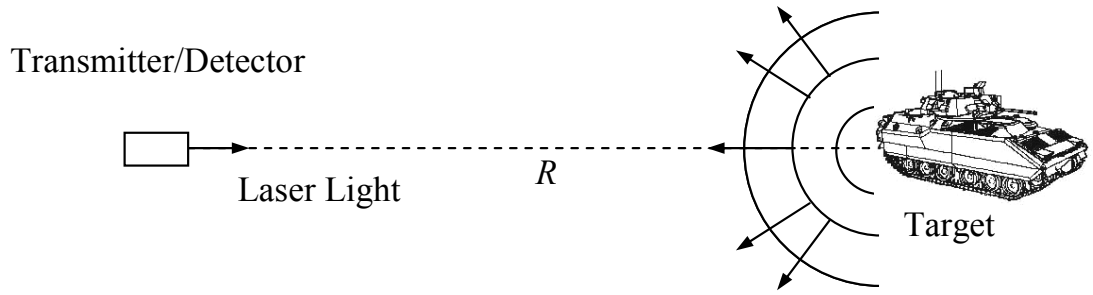

Figure 2.6 Laser light transmitted by the transmitter travels ideally straight to the target so the power detected by the detector is inversely proportional to R^2, instead of R^4 of the transmitted power.

2.4 Principle of Laser

The principle of laser is essentially a selective light amplification – only light with certain wavelength and phase is amplified (Siegman, 1986; Wilson and Hawkes, 1987). According to general physics, all materials are in their respective energy states. Energy is scalar. In other words, it can be quantitatively expressed by a number without any additional direction, such as 30^o to north, etc. So, energy is expressed such as weight, for example, the weight of a rock is 1 Kg, which has no direction. In contrast, the velocity of artillery is a vector, which has magnitude and direction.

According to quantum physics, atomic materials are in their energy states. These energy states are discrete, meaning a material can be in state A or state B, but it cannot be in a state corresponding to energy between A and B. Let us consider a material that has three energy states as shown in Fig. 2.7. The magnitudes of the three energy states are expressed by three energy levels.

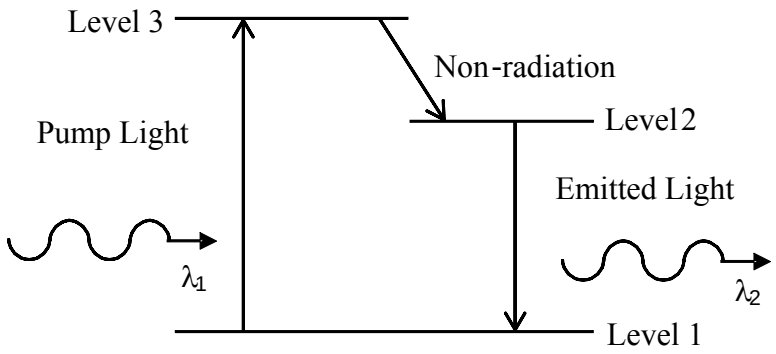

Figure 2.7 Three energy levels of a lasing material for emitting light.

The energy is stored by each electron in the form of its specific condition relative to the atomic structure or lattice of the material. An electron can be in levels 1, 2, or 3, where level 3 is higher than level 2, and level 2 is higher than level 1. The energy of electron cannot be in between levels 1 and 2, or in between levels 2 and 3.

Energy can appear in many forms. A form of energy can be transformed to another form of energy, but the sum of energy is unchanged regardless of its forms. This principle has been known as the conversation of energy. Energy can be in the form of light. A stream of light consists of photons. The magnitude of energy carried by each photon depends on the frequency of light and is defined as (Planck, 1901)

$$E = h\nu\,, \tag{2.12}$$

where ν is the frequency of light, and h is Planck's constant equal to 6.63×10^{-34} Joule×second. The relation between the frequency and the wavelength of light λ in free space is given by

$$\lambda = \frac{c}{\nu}\,, \tag{2.13}$$

Figure 2.7 shows a lasing material having three energy states which receives energy from a pump light. The pump light consists of a huge number of photons. If the energy of a photon exactly equals to the energy gap between level 3 and level 1, the energy of the photon will be absorbed by an electron at level 1, so its energy rises to level 3 and the photon disappears. The energy levels 1 and 3 are referred as the ground state and the excited state, respectively. One electron can interact with only one photon. The intensity of light indicates the number of photons. More photons in the pump light produce more electrons at the excited state, which come from the ground state.

Energy levels 3 and 2 are not stable. Electrons at energy level 3 will release their energy and thus they will arrive at energy level 2, which is the intermediate state. The energy released in this process equals to the energy gap between level 3 and level 2, and it is not in the form of light or photons. Accordingly, this process is known as a non-radiation transition. For example, the released energy is transferred to the lattice or the structure surrounding the electron. Electrons at energy level 2 will again release their energy and come back to energy level 1, which is a stable energy level. The released energy equals to the gap between level 2 and level 1, and it is in the form of light. In other words, electrons at energy level 2 decay to energy level 1 by emitting photons having specific energy. Referring to Eqs. (2.12) and (2.13), this specific energy will give specific frequency and wavelength of light.

Referring to Fig. 2.7, the gap between energy levels 3 and 1 is larger than the gap between energy levels 2 and 1. Therefore, the absorbed photon energy is larger than the emitted photon energy. In other words, the frequency of the pump light is higher than the frequency of the emitted light, and the wavelength of the pump light is

shorter than the wavelength of the emitted light. If the wavelength of the pump light is λ_1 and the wavelength of the emitted light is λ_2, then $\lambda_2 > \lambda_1$.

All emitted photons have the same energy thus the same wavelength λ_2. Each emitted photon is a wave. However, the phase of each emitted photon or wave is not necessarily uniform, since the photons are randomly emitted. This process is known as spontaneous emission. Einstein first proposed that in addition to spontaneous emission (Einstein, 1917), there must be stimulated emission. In the stimulated emission, a photon with wavelength λ_2 will stimulates an electron to emit a clone photon that is identical to the stimulating photon. The clone photon has the same wavelength, phase, and polarization as the stimulating photons. When these two identical photons pass through the lasing material again, two identical photons will generate four identical photons, and so forth. These identical photons are also called coherent photons and the emitted beam becomes a coherent beam.

2.4.1 Optical Cavity

In order to have stimulated emission, laser systems utilize an optical cavity which consists of a lasing material sandwiched by two reflectors M_1 and M_2 with a separation distance L as shown in Fig. 2.8 (Siegman, 1986). A wave propagates from left to right in the cavity. At the end of the cavity, which is reflector M_2, the wave is reflected and propagates from right to left. The two waves superimpose resulting in a standing wave in the cavity, where two nodes of the standing wave are at M_1 and M_2, respectively. To form a standing wave in the cavity, the wavelength must be

$$\frac{\lambda}{2} = nL\,, \tag{2.14}$$

where n is an integer, 1, 2, 3, 4, ….

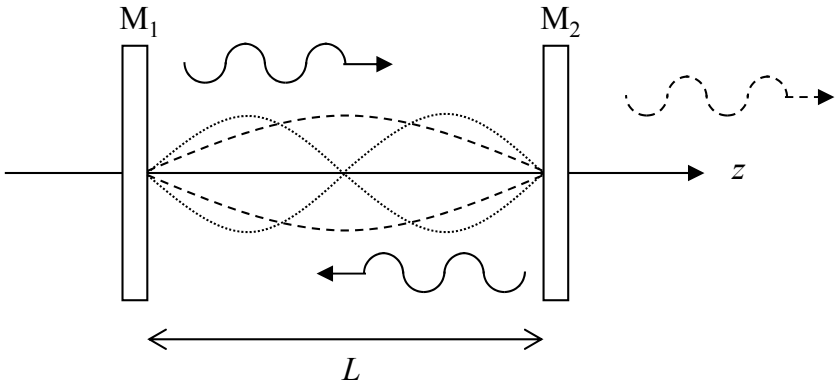

Figure 2.8 Optical cavity consisting of a lasing material sandwiched by two reflectors.

Let us now consider the lasing material emits a number of photons which are not identical to each others. In other words, the photons are not coherent or are not in phase. One of the photons propagating along the optical axis z is reflected by reflector M_2. This photon passes through the lasing materials and stimulates an identical photon or in-phase photon. Both coherent photons are then reflected by reflector M_1, passing through the material again and generate four coherent photons. In accordance with the condition of standing wave in the cavity, all four waves of four photons are in phase. In a short time a huge number of coherent photons are generated. Finally, the number of these dominant photons is much larger than spontaneous and other stimulated photons. Thus, an optical cavity provides two functions: (1) to determine precisely the lasing wavelength and (2) to select a group of identical stimulated photons. To get the light from the cavity, a reflector can be a partial reflector, for

example M_1 is a 100% mirror and M_2 is a 99% mirror, so 1% of the light is emitted through M_2.

2.4.2 Intensity of Coherent Light

A light wave representing a photon at a position in space can be expressed as (Hecht, 2002)

$$E_1 = E_{01}\sin(\omega t + \alpha_1). \tag{2.15}$$

The intensity of light is the averaged light energy over the response time, it is usually defined as follows.

$$I_1 = \frac{1}{T}\int_{\tau}^{\tau+T} |E_1|^2\, dt = \frac{1}{T}\int_{\tau}^{\tau+T} (E_{01}\sin(\omega t + \alpha_1))^2\, dt = \frac{1}{2}{E_{01}}^2, \tag{2.16}$$

where $\omega = 2\pi/T$. Assume that another photon given by

$$E_2 = E_{02}\sin(\omega t + \alpha_2), \tag{2.17}$$

is at the same position.

Its intensity is

$$I_2 = \frac{1}{T}\int_{\tau}^{\tau+T} |E_2|^2\, dt = \frac{1}{T}\int_{\tau}^{\tau+T} (E_{02}\sin(\omega t + \alpha_2))^2\, dt = \frac{1}{2}{E_{02}}^2. \tag{2.18}$$

The light wave resulting from the superposition of these two photons is

$$E = E_{01}\sin(\omega t + \alpha_1) + E_{02}\sin(\omega t + \alpha_2), \tag{2.19}$$

and its intensity is

$$I = \frac{1}{T}\int_{\tau}^{\tau+T} [E_{01}\sin(\omega t + \alpha_1) + E_{02}\sin(\omega t + \alpha_2)]^2\, dt, \tag{2.20}$$

After solving the integrations inside the squared bracket, one obtains

$$I = \frac{1}{2}{E_{01}}^2 + \frac{1}{2}{E_{02}}^2 + E_{01}E_{02}\cos(\alpha_1 - \alpha_2), \tag{2.21}$$

or

$$I = I_1 + I_2 + 2\sqrt{I_1 I_2}\cos(\alpha_1 - \alpha_2). \tag{2.22}$$

When there are N photons at the same position, the light wave resulting from N photons can be express as

$$E = \sum_{i=1}^{N} E_{0i}\sin(\omega t + \alpha_i). \tag{2.23}$$

Referring to Eq. (2.20), the intensity becomes

$$I = \frac{1}{2}\sum_{i=1}^{N}{E_{0i}}^2 + \sum_{j>i}^{N}\sum_{i=1}^{N} E_{0i}E_{0j}\cos(\alpha_i - \alpha_j). \tag{2.24}$$

For incoherent light such as natural light, the phase α_i and α_j of photons are randomly distributed such that

$$\sum_{j>i}^{N}\sum_{i=1}^{N} E_{0i}E_{0j}\cos(\alpha_i - \alpha_j) = 0. \tag{2.25}$$

Accordingly, the resulting intensity is

$$I = \frac{1}{2}\sum_{i=1}^{N}{E_{0i}}^2 = \sum_{i=1}^{N} I_i. \tag{2.26}$$

Thus, the resulting intensity is the sum of the intensity of all photons.

For coherent light such as laser light, all photons are identical. In other words, $\alpha_i = \alpha_j$, and $\cos(\alpha_i - \alpha_j) = 1$. Therefore, Eq. (2.24) becomes

$$I = \frac{1}{2}\sum_{i=1}^{N}{E_{0i}}^2 + \sum_{j>i}^{N}\sum_{i=1}^{N} E_{0i}E_{0j}, \tag{2.27}$$

which can be rewritten as

$$I = \frac{1}{2}\left(\sum_{i=1}^{N} E_{0i}\right)^2. \tag{2.28}$$

Remember that for all photons, $E_{0i} = E_0$; hence Eq. (2.26) can be written

$$I_{Incoherent} = \frac{1}{2}\sum_{i=1}^{N} {E_0}^2 = \frac{1}{2}\left(N{E_0}^2\right), \tag{2.29}$$

and Eq. (2.28) becomes

$$I_{Coherent} = \frac{1}{2}\left(\sum_{i=1}^{N} E_0\right)^2 = \frac{1}{2}\left(NE_0\right)^2. \tag{2.30}$$

For a light beam containing N photons, if the light is coherent, the intensity will be $\frac{1}{2}(NE_0)^2$. If the light is incoherent, the intensity will be $\frac{1}{2}NE_0^2$. Thus, even though both beams contain the same number of N photons, the intensity of the coherent beam is N times higher than the intensity of the incoherent beam.

Note that intensity is energy per area, so the total energy of each beam is the same. However, the coherent beam contains the light energy in a smaller area. Therefore, a laser beam has significantly higher intensity as compared with an incoherent light beam having the same power.

For illustration, we analyze a laser beam emitted from a laser pointer. In many countries, laser pointers are regulated so that their power cannot be higher than 5 mW. Assuming we have a laser pointer emitting a red laser beam having 635 nm wavelength and 3 mW optical power. According to Eq. (2.13), the light frequency is 4.72×10^{14} sec^{-1}. Then according to Eq. (2.12), the energy of a photon is 31.29×10^{-20} Joule. The power of 3 mW means 3×10^{-3} Joule/sec. Therefore, the beam is a stream of $(3\times10^{-3}/31.29\times10^{-20}) = 9.59\times10^{15}$ photon/sec. Remember that film movie frame rate is 24 frames per second, we may assume that our eye's response time is 1/24 sec. Within 1/24 sec, the eye would collect $(9.59\times10^{15}/24) = 4\times10^{14}$ photons from this laser beam. Further assuming that the laser beam is incident to a target, and only a small portion,

for example 10^{-6}, of the reflected light is collected by the eye, the number of photons will be $N = 4\times10^{8}$. Accordingly, we will see the laser light 4×10^{8} times brighter than an incoherent beam with the same power such as from a regular flash light.

2.5 Eye-Safe Laser

A schematic diagram of the elements of the human eye is illustrated in Fig. 2.9 (Hecht, 2002). The eye is almost spherical with a dimension of about 24 mm long and 22 mm across. Light is incident through the cornea, which has fixed optical power provided by its curved surface. Light emerging from the cornea passes through a chamber filled with a clear watery fluid called an aqueous humor. Behind this chamber is a crystalline lens, which has adjustable optical power provided by flexible curved surfaces. Behind the lens is another chamber filled with a vitreous humor. Finally, at the back of the eye is the retina which absorbs incident light.

The retina is sensitive to visible light having wavelength from 400 nm to 780 nm. The sensitivity of the eye to different wavelengths is a curve peaking at 555 nm, which is the central wavelength of sunlight. The eye cannot see light with wavelengths smaller than 400 nm (ultra-violet or UV light) and larger than 780 nm (infrared or IR light). However, even though the retina cannot detect UV or IR light, a high power UV or IR light incident on the retina can damage the retina temporally or permanently. Therefore, an invisible high power light beam is even more dangerous to the eye.

A person exposed to laser radiation and especially invisible radiation may be unaware that damage is occurring. Some lasers are so powerful that even the diffuse reflection from a surface can be hazardous to the eye.

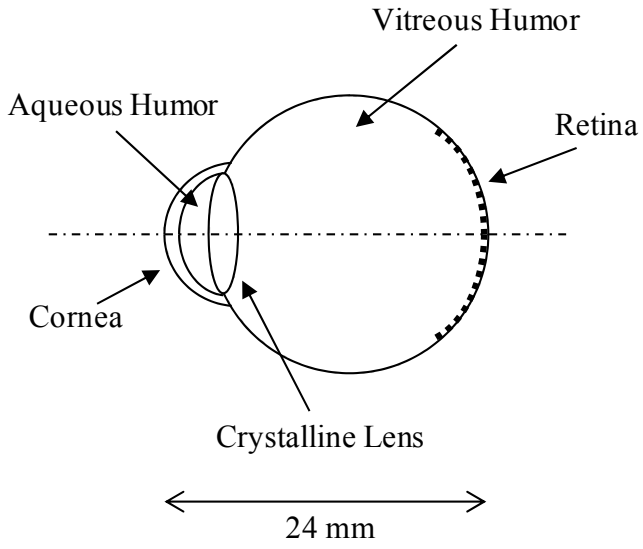

Figure 2.9 Elements of the human eye.

Laser radiation predominantly causes eye injury via thermal effects on the retina. A transient increase of only $10^{o}C$ can sufficiently destroy retina cells. The coherent laser light can be concentrated into an extremely small spot on the retina by the focusing mechanism of the eye. It was reported that an 11 year old child who temporarily damaged her eyesight by holding an approximately 5 mW red laser pointer close to the eye and staring into the beam for 10 seconds, experienced scotoma (localized damage of retina) but fully recovered after 3 months. If the laser is sufficiently powerful, permanent damage can occur within a fraction of a second, faster than a blink of an eye.

Sufficiently powerful visible to near IR laser radiation, from 400 to1400 nm, will penetrate the eye and may cause heating of the retina, whereas exposure to laser radiation with wavelengths less than 400 nm and greater than 1400 nm are largely absorbed by the cornea and the crystalline lens. IR laser light at 780-1400 nm penetrating the eye is particularly hazardous, since the body's protective reflex

response is triggered only by visible light. For example, some people exposed to high power Nd:YAG laser emitting invisible 1064 nm radiation, may not feel pain or notice immediate damage to their eyesight.

Eye safety is a serious problem when laser beams must be transmitted through the open air. So the use of lasers at wavelength 1.4 to 1.8 μm is increasing. At these wavelengths, the laser light is largely absorbed by the cornea.

Military agencies have been at the forefront of studying eye hazards and developing lasers that emit light at wavelengths that reduce eye hazards to their own troops and bystanders during training exercises, war games, and even combat. Military systems need more power, so they can benefit from shifting to the eye-safe wavelengths.

Water absorption in the eye blocks light at wavelengths longer than 1.4 μm from reaching the retina. Measured corneal absorption is close to that of water, which makes up about 70% of corneal tissue. The absorption increases steadily from 1.2 to 2.9 μm. Accordingly, lasers at eye-safe wavelengths are replacing older neodymium lasers (emitting at 1.06 μm) for LRFs. However, although high power laser light at eye-safe wavelengths may not damage retina, if the power is over the threshold, the laser light can burn the cornea. For example, at 1.4 μm, the cornea damage threshold is several Joule/cm^2 radiant exposure. Although most cornea injuries will heal, they are nonetheless “exceedingly painful and disabling.”

An example of eye-safe laser is erbium doped glass, which is often written as , solid state laser. This laser contains an active lasing rod made of. The energy levels of erbium are illustrated in Fig. 2.10. The wavelength of pumping light is 980 nm, and the wavelength of the emitted light is 1540 nm which is in the eye-safe region.

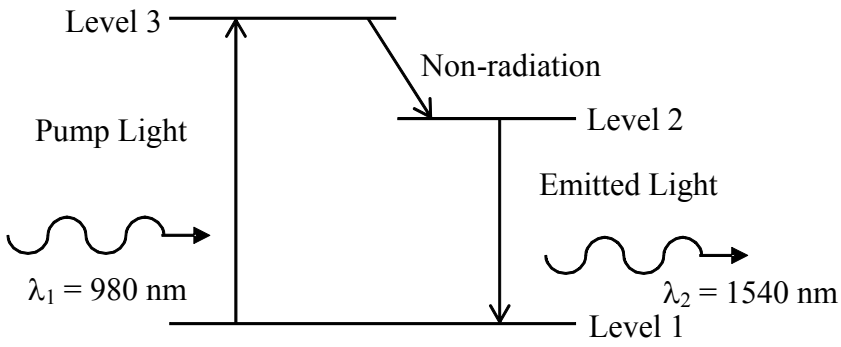

Figure 2.10 Three energy levels of an solid state laser.

A schematic diagram of an solid state laser is given in Fig. 2.11 where an Er:Glass rod functions as an active lasing medium. Both ends of the rod are polished for acting as two mirrors M_1 and M_2 of an optical cavity. Thus, the rod is an active lasing medium and also an optical cavity. The rod is illuminated from its side with pumping light provided by a laser diode (also called semiconductor laser) or several laser diodes at 980 nm wavelength. One of widely used pump light is InGaAs laser diode. The rod absorbs energy of the pumping light from its side and emits coherent light at 1540 nm from its ends according to its energy level structure. Light emitted from one end is used for transmitting to a target and the other one emitted from the other end can be detected by a photodetector as a reference for measuring the time-of-flight.

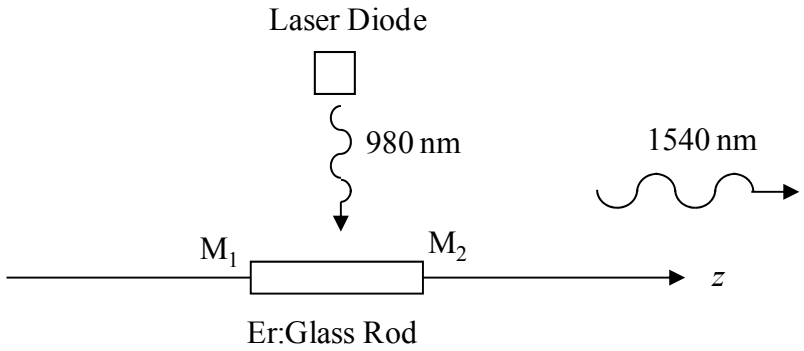

Figure 2.11 Schematic diagram of Er:Glass solid state laser.

The transmission curve of Er:Glass is shown in Fig. 2.12, which reveals that its absorption is strong (or weak transmission) at 980 nm wavelength.

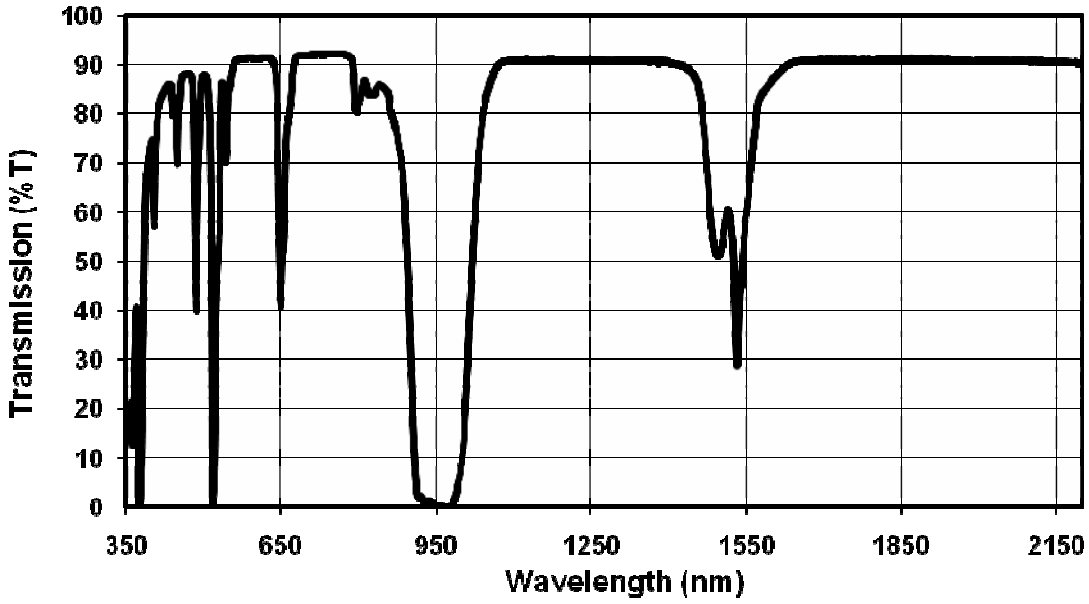

Figure 2.12 Transmission curve of Erbium (Kigre Inc.).

2.6 Optical Transmitter and Receiver

A typical handheld LRF is schematically illustrated in Fig. 2.13. It consists of a high power laser for emitting light pulses and an optical receiver that collects reflected signals from targets and at the same time views the target. Needless to say electronic parts for electronic signal processing and operation control are also included in the LRF together with battery power supply.

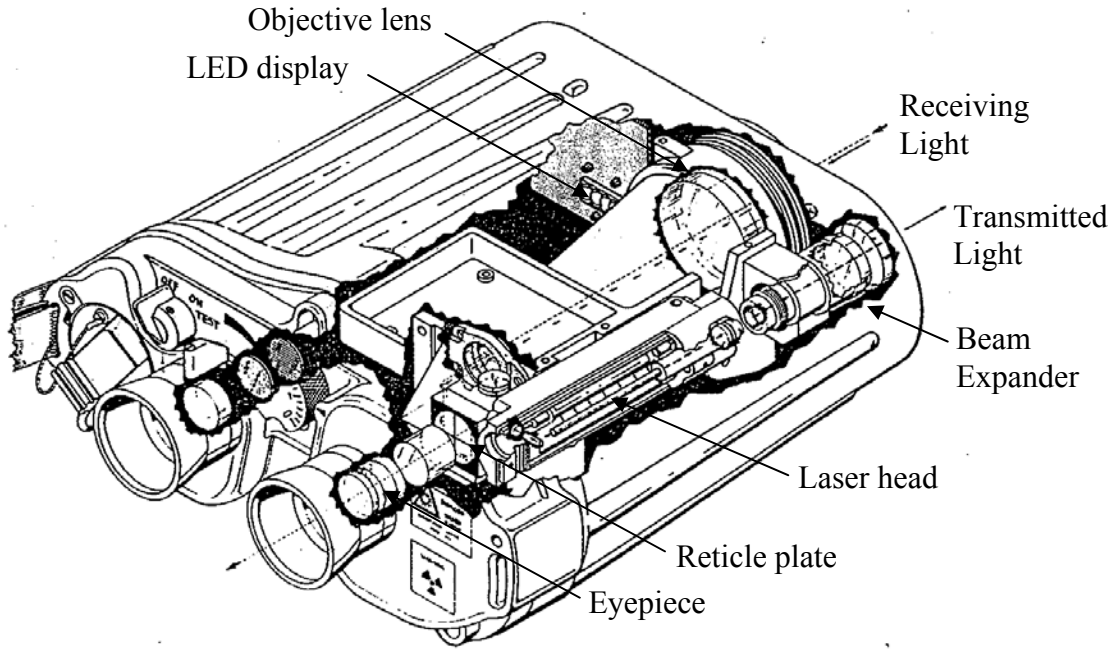

Figure 2.13 Schematic diagram of a handheld LRF (LP7 manual, Simrad Optronics**).**

2.6.1 Optical Transmitter

The transmitter of the LRF consists of a laser and a beam expander. A collimated beam emitted by the laser is expanded by the beam expander in order to

reduce its divergence. This can be done, for example, using a telescopic beam expander consisting two lenses as shown in Fig. 2.14. This beam expander is known as the Keplerian telescope (Kingslake, 1983). The beam diameter is expanded by a magnification factor (MP) of f_2/f_1, where f_1 and f_2 are the focal lengths of lenses in the telescopic beam expander. Accordingly, the divergence of the beam is reduced by a factor of f_2/f_1.

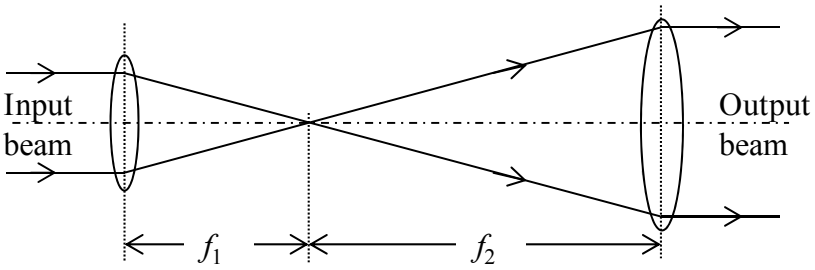

Figure 2.14 Keplerian telescopic beam expander magnifies beam waist and reduces beam divergence.

The Keplerian beam expander should only be used with low-intensity laser beams. The first input lens will focus the laser light to a very small spot at its focal point. For a pulse laser, the beam intensity is often sufficiently large to ionize the air at the focal point of the lens. This phenomenon, which looks and sounds like a spark formed between two high voltage electrodes, is known as air breakdown. It was observed first in 1963 with a Q-switched ruby laser. When air breakdown occurs, most of the energy of the laser beam is absorbed by the ionized air of the laser-produced spark. Therefore, the beam that passes through the beam expander will be attenuated and the temporal pulse shape will be distorted (Alcock *et al*., 1970).

Therefore, for a pulsed LRF the Galilean beam expander is widely used because the laser light is not focused. The Galilean telescope uses a concave (negative) lens and a convex (positive) lens. The Galilean beam expander that corresponds to the Galilean telescope is shown in Fig. 2.15, which expands the beam by the same MP of f_2/f_1. Note that to produce the same beam expansion, the Galilean beam expander is shorter than the Keplerian beam expander.

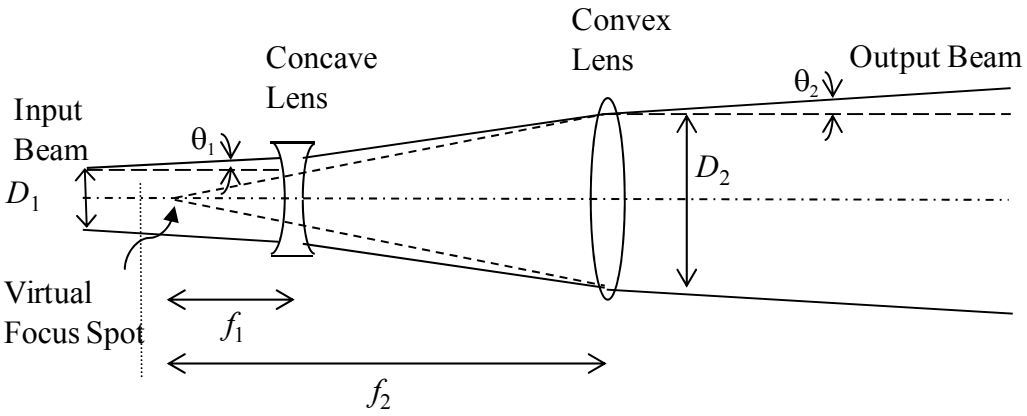

Figure 2.15 Galilean telescopic beam expander magnifies beam waist and reduces beam divergence.

2.6.2 Optical Receiver

Besides being used for receiving the reflected laser light, the receiver is also used for sighting the target through an objective lens. Since the target is very far away, the objective lens forms an image of the target on the viewing reticle as shown in Fig. 2.16 which is positioned in the focal plane of the lens. The reticle and the image of the target are viewed through the right eye piece. The objective lens and the reticle are centered on the optical axis. Instead of viewing the reticle, the left eyepiece is used to view the display showing the result of the detection, i.e., the range of the

target, and other information. Thus, it does not view the target. The operator of the LRF will see the superimposed image of the display and the reticle.

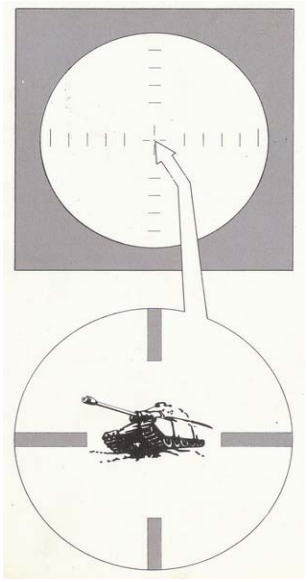

Figure 2.16 An image of the target is formed on the viewing reticle.

The optical receiver works as follows: The light received through the objective lens is divided into two paths using a beam splitter cube which contains a dichroic mirror that transmits the IR light at 1540 nm and reflects the visible light as shown in Fig. 2.17. Consequently, a visible image is formed on the reticle which is viewed through an eyepiece and IR light is directed to a detector.

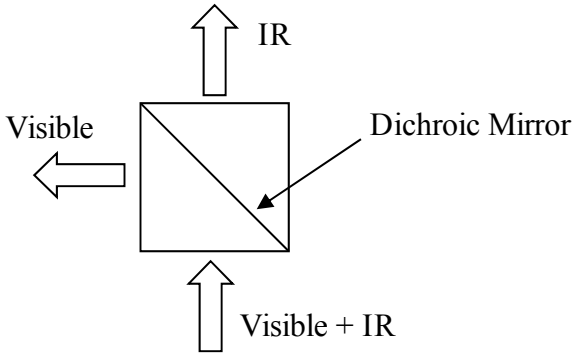

Figure 2.17 Beam splitter cube transmits the IR light and reflects the visible light.

A schematic diagram of the optical receiver is illustrated in Fig. 2.18. The visible illuminating light and the reflected IR laser light from the target are received by the objective lens. The visible and the IR images of the target are formed at the focal plane of the lens. Note that the visible and the IR focal lengths may not be the same. After passing through a prism block, the visible light is reflected toward the reticle that is mounted on the cube. The reticle is positioned at the visible focal length of the objective lens. Thus the visible image of the target is formed on the reticle. An eye piece is used for viewing the reticle together with the image of the target. The wedge prism in front of the prism block is used for fine adjustment of alignment of the optical axis. The IR light is received through the cube and directed toward a photodetector. The received IR light passes through a pinhole, which is positioned at the IR focal plane of the objective lens and a 1540 nm bandpass filter before reaching a photodetector.

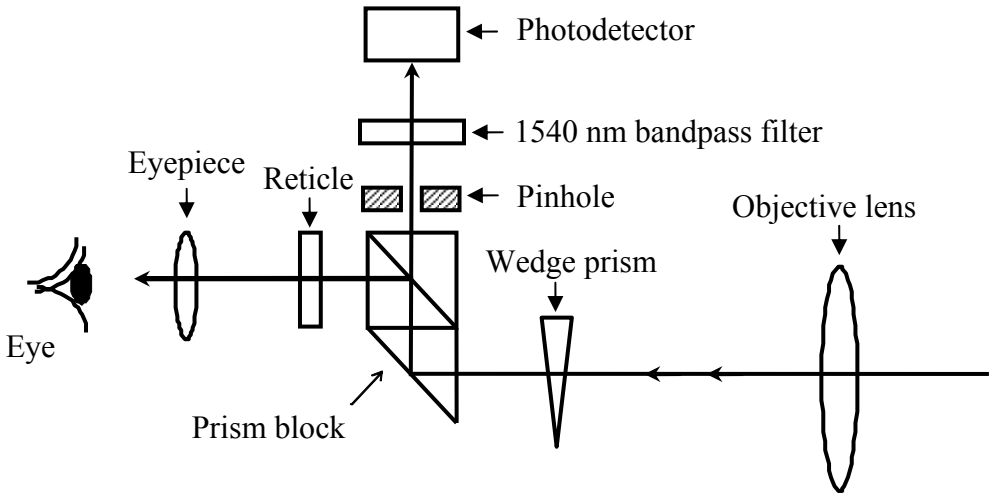

Figure 2.18 Schematic diagram of an optical receiver of LRF.

The pinhole mounted on the beam splitter cube has a diameter of 0.2 mm while the objective lens has 50 mm diameter and 155 mm focal length. Therefore, the pinhole limits the field of view of the receiver to 1.3 mrad. It means, at 1 Km target distance, the pinhole will allow the light reflected from a target with diameter 1.3 m to be detected.

In an older rangefinder system, to obtain the reference start pulse, a part of the transmitted laser light is reflected toward and input into the prism block in Fig. 2.18. The start pulse is used as a reference to measure the time of flight of the laser pulse. In current system, optical start pulse is no longer needed because the laser has its own detector to detect the start pulse. The reference for measuring the transit time of the laser pulse is provided by an electronic signal.

The prism block consists of the beam splitter cube and prisms that are Porro prism and a right angle prism as shown in Fig. 2.19. The elements are: (1) right angle prism, (2) surface of the right angle prism facing the incoming light which is coated

by broadband anti-reflection, (3) Porro prism, (4) beam splitter cube, (5) multilayer dichroic mirror, (6) reticle, (7) bottom side of the beam splitter cube, where a pinhole is aligned with the center of the reticle which is the focal point of the objective lens.

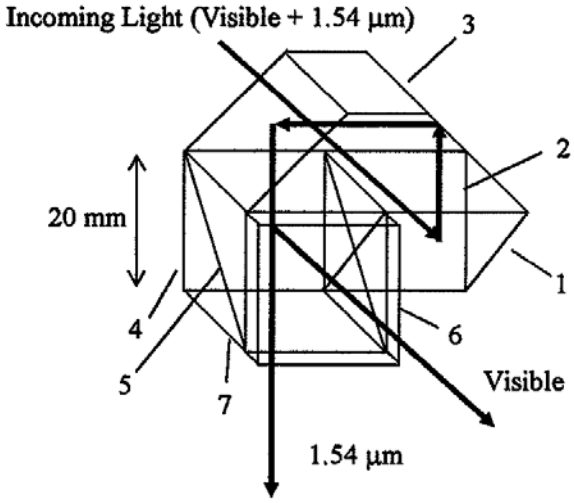

Figure 2.19 3-dimensional diagram of prism block in the optical receiver.

The incoming light focused by the object lens enters surface (2) of the right angle prism (1). The light experiences internal reflection in the right angle prism (1) and enters the Porro prism (3). The light further experiences twice internal reflections in the Porro prism (3) and enters the beam splitter cube (4). At the middle layer of the beam splitter cube (4), which is the multilayer dichroic mirror (5), the light is divided into visible light and 1540 nm IR light. The IR light is transmitted through the beam splitter cube (4) to its bottom (7) and passes through a pinhole. The visible light is reflected by the dichroic mirror (5) and forms the image of the target on the reticle (6) which is viewed through an eye piece. The IR light passing through the pinhole is detected by a photodetector.

The visible light which is reflected four times in the prism block provides an erected image on the reticle, such as two Porro prisms provide an erected image in a binocular. Thus, the prism block functions as an erecting system in the LRF, in addition to the separation of the IR laser light from the visible image.

CHAPTER III

GAUSSIAN BEAM RANGE EQUATION

As discussed in Chap. II, the reason of using laser for range finding is that a laser can emit high power light which is almost collimated with a small beam divergence, typically in the order of milliradian. Therefore, with respect to the range to be measured, beam size of the transmitted laser may be either totally or partially reflected by the target. In this chapter, the range equation for these two conditions is discussed. It is found that there is discrepancy between detected powers of light pulse partially and totally reflected by targets. To overcome this problem, we propose a new range equation which takes into account Gaussian profile of laser light. We also introduce a new operation coefficient for estimating the returned powers in LRF as an empirical correction factor.

3.1 Geometrical Range Equation

Figure 3.1 shows a schematic diagram of the range measurement by LRF when the transmitted beam is totally reflected by the target. In order to measure the time of flight, an objective lens with diameter D is used to collect the reflected light onto a photodetector. If the transmitted beam is totally reflected by the target (e.g., R is small), we have

$$P_{Target} = P_{Transmitter} , \tag{3.1}$$

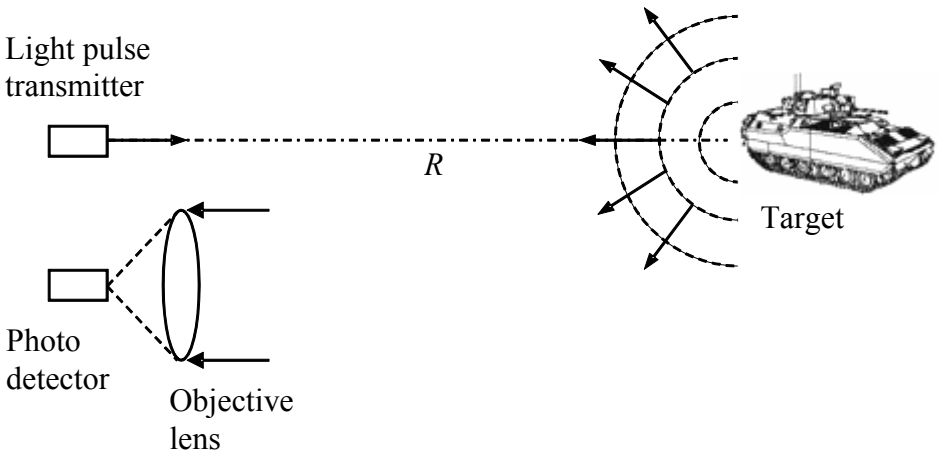

Figure 3.1 Reflected laser light is collected by an objective lens.

By regarding the lens diameter as the detector area and taking Eq. (3.1) into account, Eq. (2.7) can be rewritten as

$$P_{Detector} = \pi\left(D/2\right)^2 \times \frac{P_{Target}}{2\pi R^2}$$

$$= \frac{D^2}{8R^2} \times P_{Transmitter} \tag{3.2}$$

However, in many cases of long range measurement, the transmitted laser beam diverges such that its diameter becomes larger than the target dimension. Consequently, the beam is only partially reflected by the target as shown in Fig. 3.2. In this case, the target reflects only a portion of the transmitted power.

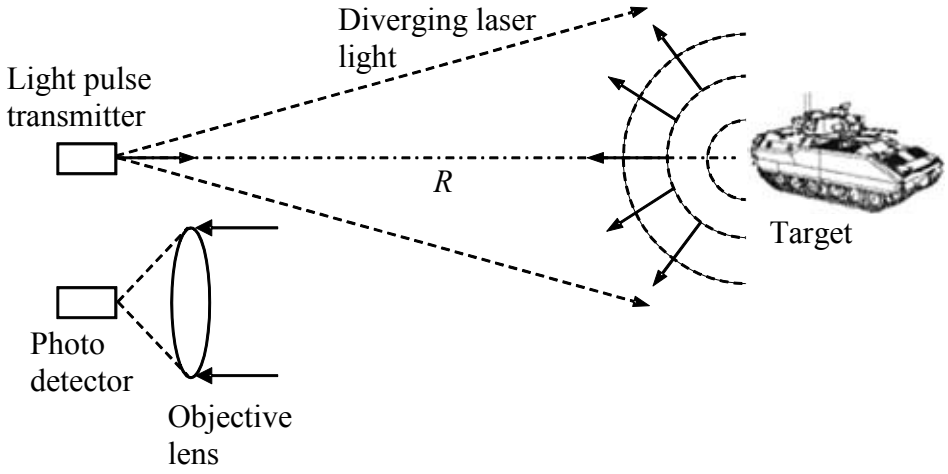

Figure 3.2 Transmitter emits diverging beam toward target.

Assume that the transmitted light has a half angle of beam divergence θ. For small θ, the area covered by the light cone at distance R is $\pi(\theta R)^2$ as shown in Fig. 3.3.

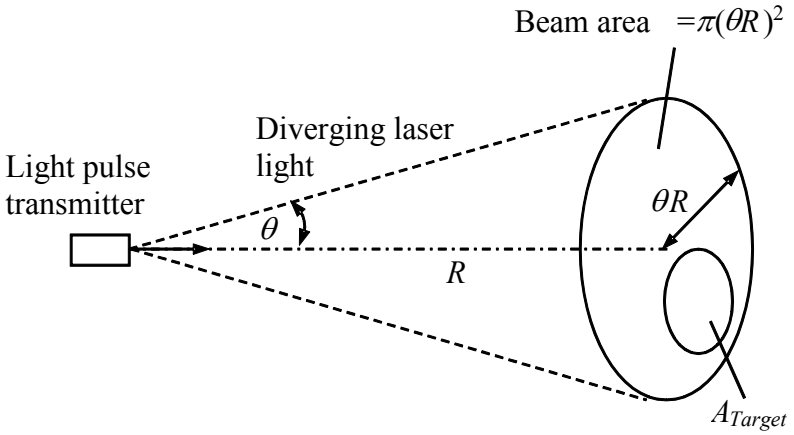

Figure 3.3 The area covered by the light cone is $\pi(\theta R)^2$.

The power reflected by the target can be written as

$$P_{Target} = \frac{A_{Target}}{\pi\theta^2 R^2} \times P_{Transmitter} \,. \tag{3.3}$$

where A_{Target} is the area of the target that reflects the transmitted light beam. As a consequence, Eq. (3.2) becomes

$$P_{Detector} = \frac{D^2}{8R^2} \times \frac{A_{Target}}{\pi\theta^2 R^2} \times P_{Transmitte\,r}$$

$$= \frac{D^2 A_{Target}}{8\pi\theta^2 R^4} \times P_{Transmitter}\,. \tag{3.4}$$

It should be noticed that we have assumed that the transmitted power is evenly distributed in a cone. Actually, the light beam is a Gaussian beam, which has peak intensity at the center.

In the above discussion, we have actually assumed that the target is a diffuse object that is subject to Lambert's law (Moller, 1988) and its plane is parallel to the LRF. This implies that the transmitted and the reflected light pulses impinge perpendicularly on the target and the detector, respectively. If the angle between the transmitted beam and the normal of the reflecting target is φ, the reflected power must be multiplied with $\cos\varphi$. Note that for intensity, it must be $0 \le \cos\varphi \le 1$, or $-90^o \le \varphi \le 90^o$. According to the cosine law of Lambert, Eq. (3.4) must be multiplied with $\cos\varphi$, which is the angle between the transmitted beam and the normal of the target

$$P_{Detector} = \frac{D^2 A_{Target}}{8\pi\theta^2 R^4} \times P_{Transmitter} \times \cos\varphi\,. \tag{3.5}$$

The overall resultant value of $\cos\varphi$ may be approximated by 0.5, because the target does not have a flat surface but a topographical structure. Accordingly, Eq. (3.5) reduces to

$$P_{Detector} = \frac{D^2 A_{Target}}{16\pi\theta^2 R^4} \times P_{Transmitter}\,. \tag{3.6}$$

3.2 Physical Range Equation

For actual power detection, the geometrical range equation given in Eq. (3.6) needs to include physical attenuating coefficients such as: target reflectance ρ; optical efficiency of the transmitter $\eta_{Transmitter}$; optical efficiency of the receiver $\eta_{Receiver}$; and atmosphere transmission factor given by

$$T = e^{-\alpha R}, \tag{3.7}$$

where α is the atmosphere extinction coefficient due to absorption and scattering. Consequently, the physical range equation for a partially reflected target can be rewritten as

$$P_{Detector} = \frac{T^2 \rho \eta_{Transmitter} \eta_{Receiver} D^2 A_{Target}}{16\pi\theta^2 R^4} \times P_{Transmitter}. \tag{3.8}$$

Whereas in accordance with Eq. (3.2), the physical range equation for the totally reflected target becomes

$$P_{Detector} = \frac{T^2 \rho \eta_{Transmitter} \eta_{Receiver} D^2}{16R^2} \times P_{Transmitter}. \tag{3.9}$$

Equations (3.8) and (3.9) are widely known range equations in LRF (Stitch, 1972; Forrester and Hulme, 1981).

3.3 Gaussian-Beam Range Equation

When a laser beam leaves an optical cavity containing a lasing material, its beam has a Gaussian profile (Saleh and Teich, 1991). Let us consider a Gaussian beam propagating in free space along the z direction from $z = 0$. At $z = 0$, the beam waist or beam radius will be at a minimum value w_0. At a large distance z, the beam waist is approximately given by

$$w(z) = \theta z\,, \tag{3.10}$$

where θ is the half angle of the beam divergence defined as

$$\theta = \frac{\lambda}{\pi w_0}, \tag{3.11}$$

with λ is the wavelength of light.

Since the emitted laser beam has a Gaussian shape, the laser beam cannot be an ideally collimated beam. The beam is characterized by its half angle θ or full angle of divergence 2θ. As indicated in Eq. (3.11), a small beam waist w_0 will produce a large beam divergence θ, and a large beam waist will produce a small beam divergence. Note that the beam waist is the position where the intensity is $1/e^2$ of the center peak intensity.

Assume now that the target we deal with is a circular object with a radius r_{Target}. The target is located at the center of the Gaussian transmitted beam as shown in Fig. 3.4.

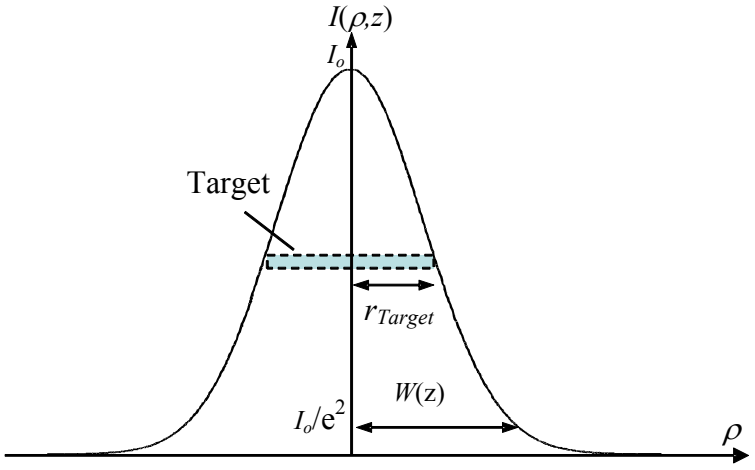

Figure 3.4 Target having radius r_{Target} at the center of Gaussian beam.

The intensity distribution of the Gaussian beam $I(\rho,z)$ is defined as (Saleh and Teich, 1991)

$$I(\rho,z)=\frac{2P_{Beam}}{\pi w^2(z)}\exp\left[-\frac{2\rho^2}{w^2(z)}\right], \tag{3.12}$$

where P_{Beam} is the total power carried by the beam given by

$$P_{Beam}=\int_0^{\infty} I(\rho,z)2\pi\rho d\rho\,. \tag{3.13}$$

The power contained within a circle of radius r_{Target} is

$$P_{Target}=\int_0^{r_{Target}} I(\rho,z)2\pi\rho d\rho$$

$$=P_{Beam}\left\{1-\exp\left[-\frac{2r_{Target}^2}{w^2(z)}\right]\right\}. \tag{3.14}$$

By referring to Eq. (3.10), for large z, such that $z = R$, the beam waist at this distance can be expressed as $w(z)=\theta R$. Thus, Eq. (3.14) becomes

$$P_{Target}=P_{Beam}\left\{1-\exp\left[-\frac{2r_{Target}^2}{\theta^2R^2}\right]\right\}. \tag{3.15}$$

Since P_{Beam} is $P_{Transmitter}$, Eq. (3.15) can be rewritten as

$$P_{Target}=P_{Transmitterr}\left\{1-\exp\left[-\frac{2r_{Target}^2}{\theta^2R^2}\right]\right\}. \tag{3.16}$$

Now we recall Eq. (3.8) and replace

$$\frac{A_{Target}}{\pi\theta^2R^2}$$

with

$$\left\{1-\exp\left[-\frac{2r_{Target}^2}{\theta^2 R^2}\right]\right\}.$$

This yields

$$P_{Detector}=\frac{T^2\rho\eta_{Transmitter}\eta_{Receiver}D^2}{16R^2}\times\left\{1-\exp\left[-\frac{2r_{Target}^2}{\theta^2 R^2}\right]\right\}\times P_{Transmitter} \qquad (3.17)$$

which is the new Gaussian beam range equation that has never been reported before.

3.4 Analysis of Range Equations

We have assembled an eye-safe LRF using MK81 Er:Glass laser from Kigre Inc. (USA) as the transmitter. The emitted laser energy and the pulse width were 3 mJ and 9 ns, respectively. Accordingly, the maximum power of $P_{Transmitter}$ was 0.33 MW. The raw full-angle of divergence of the laser beam was 4.2 mrad. After passing through 4× Galilean beam expander, the full angle of divergence should be 1.1 mrad. However, from real measurement, we found that the full angle of beam divergence was 1.2 mrad. Thus its half-angle θ was 0.6 mrad. The diameter of the objective lens D was 45 mm. Also from real measurements, we found that the transmitter optical efficiency $\eta_{Transmitter}$ was 0.85, and the receiver optical efficiency $\eta_{Receiver}$ was 0.45.

Some other data were obtained from standard references. The atmospheric absorption coefficient α is 0.1 km^{-1} at clear sky, i.e., visibility 23.5.km. The target reflectance ρ is 0.21 for a green color tank, and the target area is 2.3×2.3 m^2 according to NATO standard. For the Gaussian beam range equation, we assumed that r_{Target} = 1.15 m (half of 2.3 m).

We are now in a position to compare three range equations, Eqs. (3.8), (3.9) and (3.17) using numerical data mentioned above. Figure 3.5 shows logarithmic plots

of the detected powers as a function of the range R. Equation (3.17) is represented by a solid curve, while Eqs. (3.8) and (3.9) are dot and dash curves, respectively. The three plots show the nonlinear relationship between the returned power and the measured range. However, it appears that the detected power obtained using Eq. (3.8) is erratic, i.e., when the range is short such that the target area is larger than the light cone, the detected power becomes unrealistically large. Since the target area is 2.3×2.3 m^2 and the half angle divergence is 0.6 mrad, at R = 1.9, the beam diameter will be about the same as the target width. For R is smaller than 1.9, Eq. (3.8) produces misleading results, while Eqs. (3.17) and (3.9) are very close. On the contrary, for R is larger than 1.9, Eq. (3.9) will produce misleading results. It deviates from the plot of Eq. (3.17) which is approximately the same as that of Eq. (3.8). Therefore, it is interesting to note that Eq. (3.17) of the Gaussian beam range equation produces correct results for all values of the measured range R.

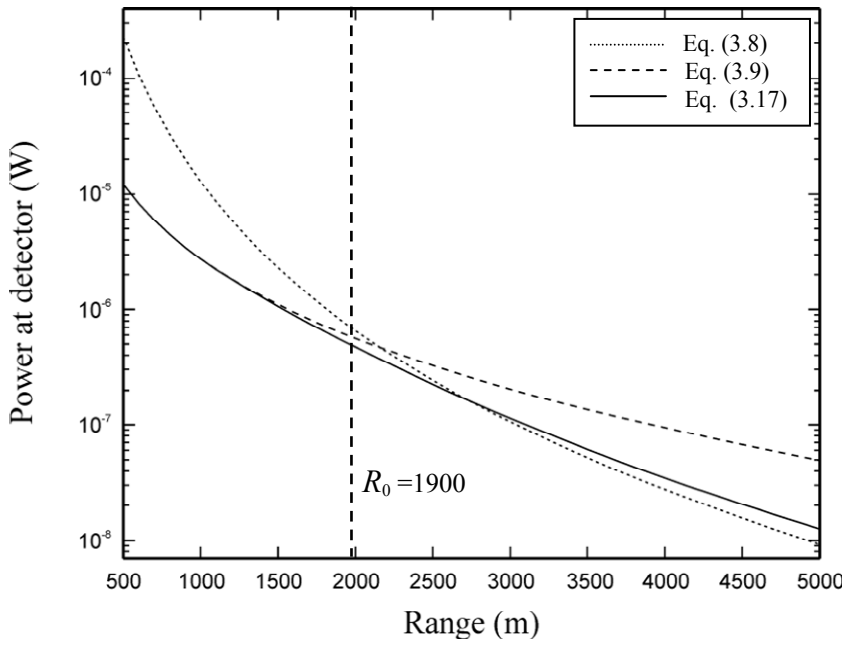

Figure 3.5 Logarithmic plot of the calculated powers as a function of the range R.

In conclusion, Eq. (3.8), a well known range equation, is valid only for large R or $R > R_o$, and Eq. (3.9), another well known range equation, which is valid only for small R or $R < R_o$, where R_o is the range where the transmitted light beam is approximately as large as the target. However, Eq. (3.17) of the Gaussian beam range equation, which has never been reported before, is valid for all values of R. The advantage of using the Gaussian beam range equation is that we do not need to check its validity by evaluating the target area and the beam diameter as required by conventional range equations of Eqs. (3.8) and (3.9).

3.5 Defining Operational Coefficient

Although we may find accurate D, θ, $\eta_{Transmitter}$ and $\eta_{Receiver}$ from real measurements of LRF, we may not accurately estimate T or α, ρ, and A_{Target} for range equations. In addition, we have approximated the overall resultant of Lambertian coefficient cosφ by 0.5. This may not be correct depending on the shape of the target. Thus, to get a correct detected power, we propose, for the first time, to modify the range equations with a correcting factor, which we call an operational coefficient or ***C***. Accordingly, Eq. (3.8) becomes

$$P_{Detector} = C \times \frac{T^2 \rho \eta_{Transmitter} \eta_{Receiver} D^2 A_{Target}}{16 \pi \theta^2 R^4} \times P_{Transmitter}, \tag{3.18}$$

where ***C*** is typically between 0 and 1. It is important to note that although the transmitted beam is perfectly aligned with the optical receiver, ***C*** may not be 1.

Equation (3.18) is applied when the target is smaller than the light beam, or the target reflects partially the transmitted beam. In the case of total reflection of the beam, i.e., the target is larger than the light beam, the detected power is

$$P_{Detector} = C \times \frac{T^2 \rho \eta_{Transmitter} \eta_{Receiver} D^2}{16R^2} \times P_{Transmitter}, \tag{3.19}$$

where the detected power is independent of the target area. Finally, for the Gaussian beam range equation, the detected power becomes

$$P_{Detector} = C_{GB} \times \frac{T^2 \rho \eta_{Transmitter} \eta_{Receiver} D^2}{16R^2} \times \left\{1 - \exp\left[-\frac{2r_{Target}^2}{\theta^2 R^2}\right]\right\} \times P_{Transmitter}, \tag{3.20}$$

Note that here the operational coefficient is denoted by $\boldsymbol{C_{GB}}$ in order to distinguish from $\boldsymbol{C}$ in Eqs. (3.18) and (3.19), where GB stands for Gaussian beam.

Let us consider that the reflected light pulse is detected by Analog Module Inc. model 759 LRF receiver module having minimum detectable power of 30 nW. The range can be measured provided the detector receives at least 30 nW of optical power. Therefore, the operational coefficient $\boldsymbol{C_{GB}}$ can be obtained from

$$C_{GB} = \frac{30 \times 10^{-9}}{\frac{T^2 \rho \eta_{Transmitter} \eta_{Receiver} D^2}{16R^2} \times \left\{1 - \exp\left[-\frac{2r_{Target}^2}{\theta^2 R^2}\right]\right\} \times P_{Transmitter}}, \tag{3.21}$$

where the returned optical power detected by this receiver is calculated using the Gaussian beam range equation of Eq. (3.17) for different maximum detectable target ranges. Table 1 shows the variation of $\boldsymbol{C_{GB}}$ as a function of maximum detectable range R which is computed by using data from real measurements and standard references or approximation. The determination of $\boldsymbol{C_{GB}}$ from real measurement is needed for later use in calibrating or correcting the range equation which is shown in the last row of the table.

The proposed operational coefficient $\boldsymbol{C_{GB}}$ or $\boldsymbol{C}$ is an empirical factor. It is useful for correcting estimation of the detectable range of similar targets, because there are uncertainties in determining atmospheric attenuating factor; reflectivity, size

and shape of the target that affects the Lambertian coefficient. It may also include the correction for misalignment between the transmitter optics and the receiver optics. In other applications, a reference target such as a circular plane with known reflectivity and radius can be employed in a test. The resulting operational coefficient $\boldsymbol{C_{GB}}$ indicates the quality of the laser range finder.

Table 3.1 Operational coefficient $\boldsymbol{C_{GB}}$ for correction of estimation of the returned power of a laser range finder.

Maximum detectable range R (km)	0.5	1.0	2.0	3.0	4.0
$P_{Detector}$ (W) before correction	1.214×10^{-5}	2.745×10^{-6}	4.726×10^{-7}	1.141×10^{-7}	3.469×10^{-8}
$\boldsymbol{C_{GB}}$	0.0025	0.01	0.06	0.26	0.87
$P_{Detector}$ (W) after correction	3×10^{-8}	3×10^{-8}	3×10^{-8}	3×10^{-8}	3×10^{-8}

CHAPTER IV

CONSTRUCTION OF EYE-SAFE LASER RANGE FINDER

In this chapter, the construction of the proposed eye-safe LRF is discussed. A block diagram of the constructed eye-safe LRF system is given in Fig. 4.1. The system consists of three main parts that are (1) laser pulse transmitter, (2) receiver, and (3) electronic counter and controller.

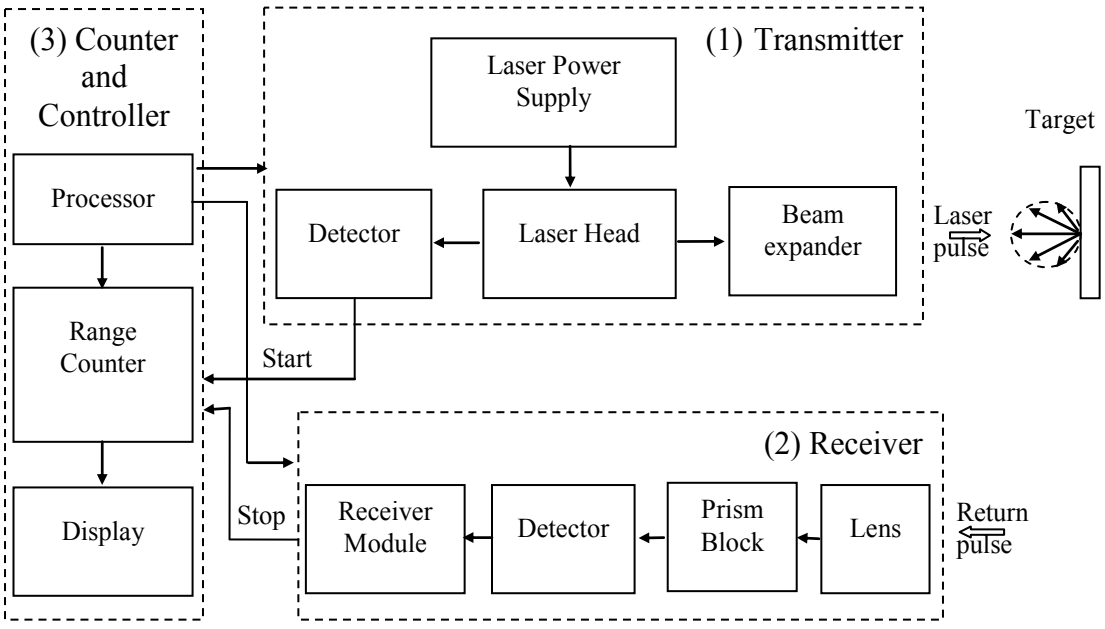

Figure 4.1 Block diagram of the constructed eye-safe LRF.

4.1 Laser Pulse Transmitter

The function of the laser pulse transmitter is to generate a high peak power laser pulse with small beam divergence and to send the pulse to the target. The narrower the pulse width, the better the accuracy of the system will be. The transmitter part consists of a laser head, a power supply module, and a beam expander.

4.1.1 Laser Head

Figure 4.2 shows a diagram of the laser head MK81 which is a diode pumped solid state laser, manufactured by Kigre Inc., USA. Its lasing medium is Er: Glass (Erbium doped glass) rod. The rod placed within a cavity made from a high reflective (HR) mirror with 99% reflectance and a coupler mirror or partial mirror which is side pumped by InGaAs laser diode operating at wavelength 980 nm. Upon the absorption of the pump light, the Er: Glass rod emits light from both ends of the rod at 1540 nm. Hence, it is suitable for eye-safe operation. A Q-switch cell (Saleh and Teich, 1991) made of Co:Spinel is placed in front of the coupler mirror. When the Q-switch is off, Co:Spinel absorbs light so that the lase oscillation cannot begin. The population inversion that is the increase of the number of electrons in the upper energy state, continues to build up until the Q-switch is turned on and Co:Spinel transmits light. When the Q-switch is turned on, a narrow laser pulse with megawatts order of power is generated and emitted from the coupler mirror. The laser output has approximately 9 ns pulse width and 3 mJ of energy. Its beam divergence is 3.5 mrad. A small portion of light is emitted from the HR mirror, which is directly detected by a photodiode. The signal from this detector is used as the start pulse signal in computing the transit time of the laser pulse.

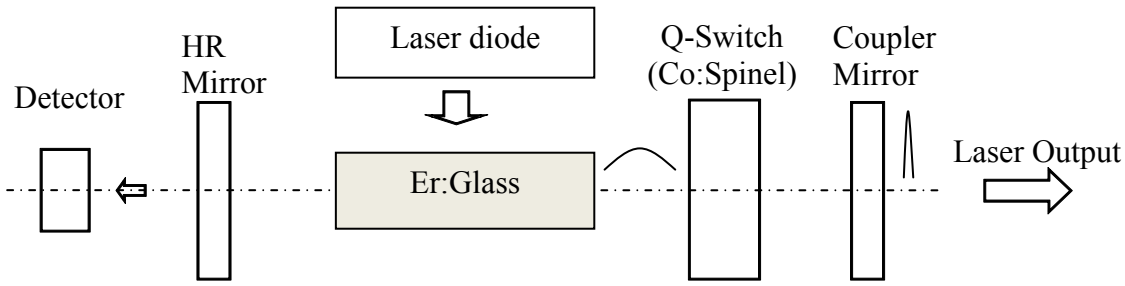

Figure 4.2 Block diagram of a laser head (Er:Glass laser).

4.1.2 Laser Power Supply

The main goal of the laser power supply is to provide extremely regulated current to the laser diode module. Because the laser input is an array of diode bars (a series/parallel combination) the power supply must provide enough voltage to forward bias the diodes. Once this voltage is exceeded, current will begin to flow. The driver must then regulate this current (typically 90 amps for the Kigre MK81) to provide proper laser output. Over voltage and/or over-current conditions will easily destroy laser diodes, so the driver must be very stable and reliable. The driver must be able to provide enough energy to the laser for each laser pulse (typically 1J for the MK81). The block diagram of the laser power supply module is shown in Fig. 4.3.

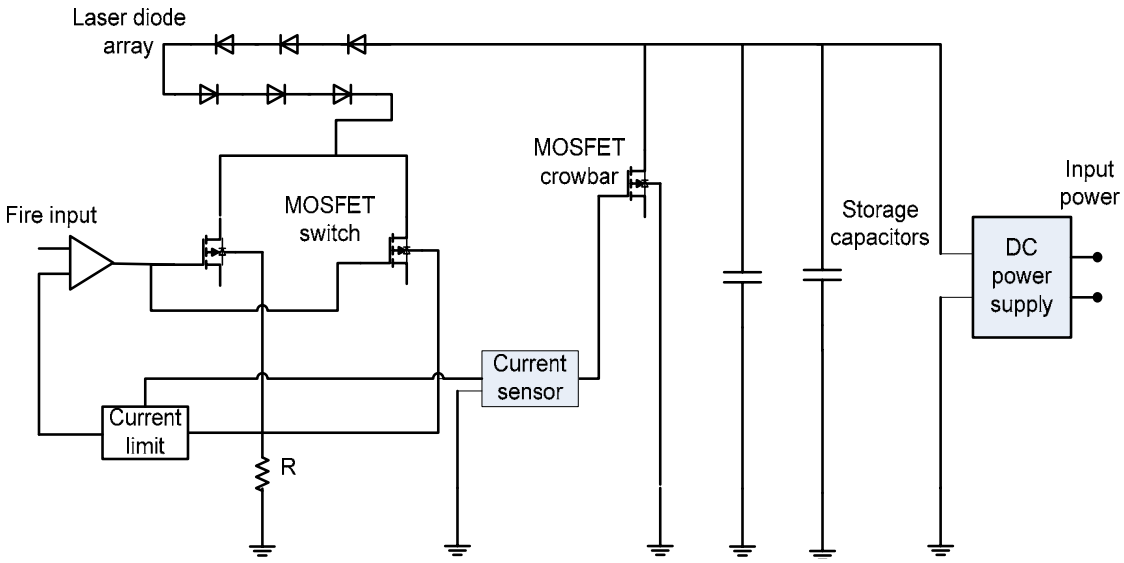

Figure 4.3 Circuit of a laser power supply module.

A power conditioning unit (DC power supply) converts battery power from 6 V to 24 V. In order to avoid current surges from the DC power supply during the nominally 200 μs-long pump pulse, energy is stored in electrolytic capacitors. Connected parallel to the capacitors is a string of laser diode bars, two MOSFETs and a small series resistor for current sensing. The function of the MOSFET is to generate the desired current waveform by switching the diode current on and off and by providing current control by means of a current sensing feedback loop. The MOSFETs are switched on and off by input pulses from a timing circuit. The third MOSFET acts as a fast crowbar circuit that senses excess current, duty cycle and temperature to prevent the diode array against damage caused by catastrophic failure of an array or the driver itself.

4.1.3 Beam Expander

The laser beam expander is for decreasing the laser beam divergence at large distances. The beam expander yields a beam that is not only larger in diameter, but also highly collimated. The result is a smaller beam diameter at a large distance when compared to the laser beam without the beam expander. Thus, the power density of laser beam incident on the target is increased, and hence better returned power to the system can be provided. Note that according to the diffraction physics, the larger beam diameter at the transmitter will produce smaller beam diameter at the target, and vice versa.

As discussed in Chapter II, the advantages of the Galilean beam expander over the Keplerian are twofolds: (1) the Galilean design contains no internal focal point and (2) the overall length of the Galilean as compared to a similar power Keplerian design is shorter. Hence, we employ the Galilean beam expander to maintain Gaussian beam profile and its power. The design diagram of the Galilean beam expander and its housing are shown in Fig. 4.4. In the design, we use a negative lens with 5.6 mm focal length and a positive lens with 28.49 mm focal length and put each lens in difference housing as in Fig. 4.4 for ease of adjustment. Since the MP of this beam expander is 5 times, it can reduce the raw beam divergence of a laser from 3.5 mrad to 0.7 mrad. The total length of the collimator after assembled and adjustment is 30 mm. The diameter of an entrance side diameter is 4 mm, while that of the exit side is about 14 mm.

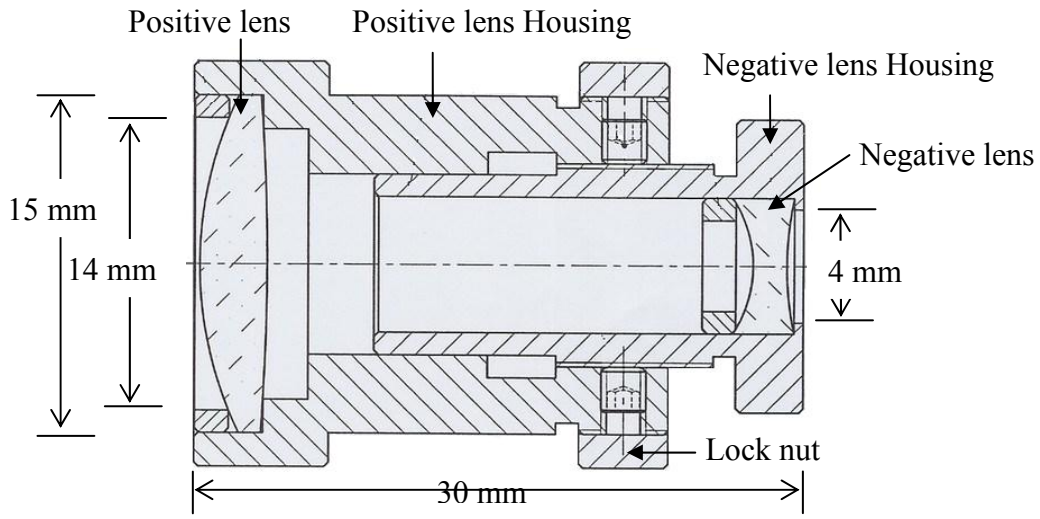

Figure 4.4 Design diagram and drawing of the beam expander mechanical housing.

A photograph of the assembled laser transmitter is shown in Fig. 4.5, which consists of the laser head, the Galilean beam expander, and the laser power supply board. Furthermore, a photograph of an oscilloscope display showing the transmitted pulse having 9 ns FWHM (full width half maximum) is depicted in Fig. 4.6. The top signal corresponds to the current signal applied to the pump laser diode, while the lower one is the laser output signal emitted from the transmitter.

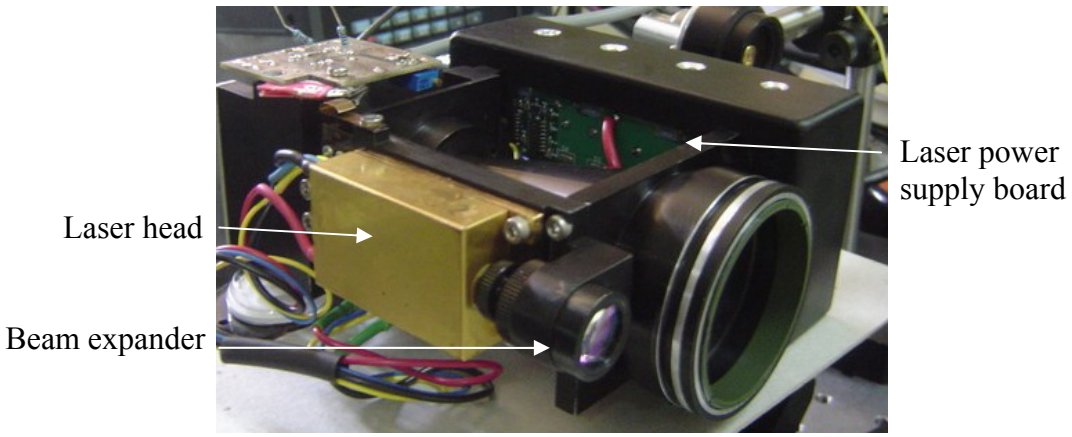

Figure 4.5 Assembled transmitter which consists of laser head, power supply, and beam expander.

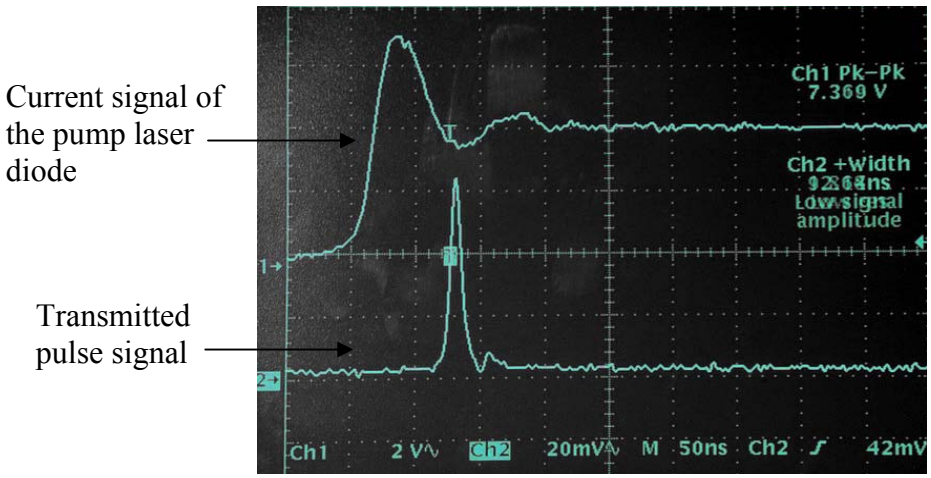

Figure 4.6 Transmitted laser pulse having 9 ns width.

4.2 Receiver

LRF receiver system consists of two main sections: (1) optical receiver and (2) electronic receiver. The optical receiver serves two functions that are to provide accurate sighting onto the target and to collect the reflected laser light onto the photodiode of the receiver.

4.2.1 Optical Receiver

On the basis of the receiver system discussed in Chapter II, we have assembled the optical receiver system whose photograph is shown in Fig. 4.7. The optical system consists of the objective lens to collect all light (visible and IR laser light), prism block (right-angle prism, Porro prism, cube beam splitter, and reticle) to separate visible light from IR laser light, pinhole to control the receiver field of view (FOV), IR-pass filter to reduce background noise and eyepiece.

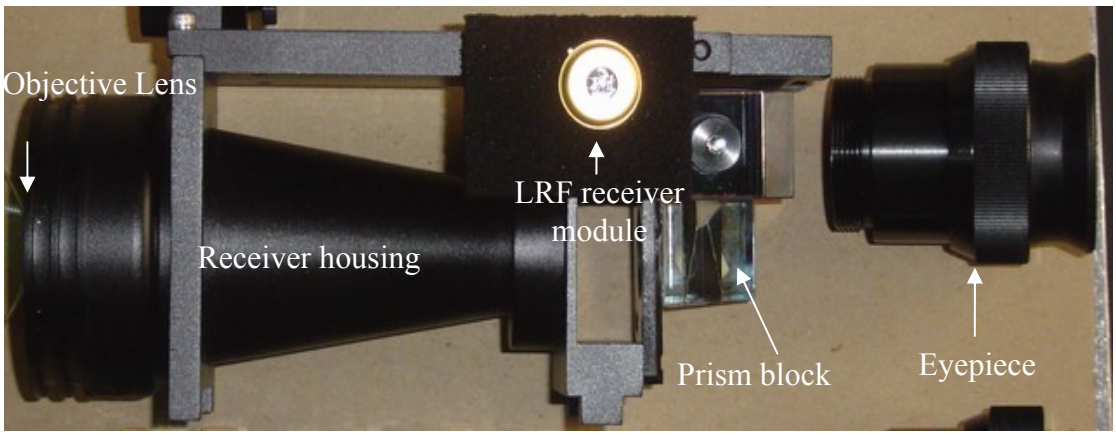

Figure 4.7 Optical receiver in the assembled unit.

The objective lens has a focal length of 155 mm (for visible light) and 158 mm for IR light with diameter of 47 mm. The eyepiece has a focal length of 26 mm with apparent 50 degree FOV. When it is combined with the objective lens to form a telescope, its magnification is 7 times with 7 degree FOV.

4.2.2 Electronic Receiver

As for the electronic receiver, a high sensitive detector module, series 759 from Analog Module Inc., USA is employed to convert a photon signal of the returned light pulse from the target to an electrical analog signal. A block diagram of the electronic receiver is shown in Fig. 4.8. It includes (1) a detector that is InGaAs PIN photodiode; (2) a trans-impedance type preamplifier for amplifying the converted electrical signal generated by the detector; (3) a band shaping or a low-pass filter whose bandwidth is determined to optimize a signal-to-noise ratio (SNR) based on the output laser pulse width and noise characteristics of the detector and the preamplifier; (4) a postamplifier which further amplifies the signal from preamplifier; (5) a

threshold control or comparator to perform threshold detection by comparing the signal amplitude from postamplifier to the threshold level that can be adjusted for false alarm rate; and (6) a pulse shaper to shape the signal suitable for the next counter circuit.

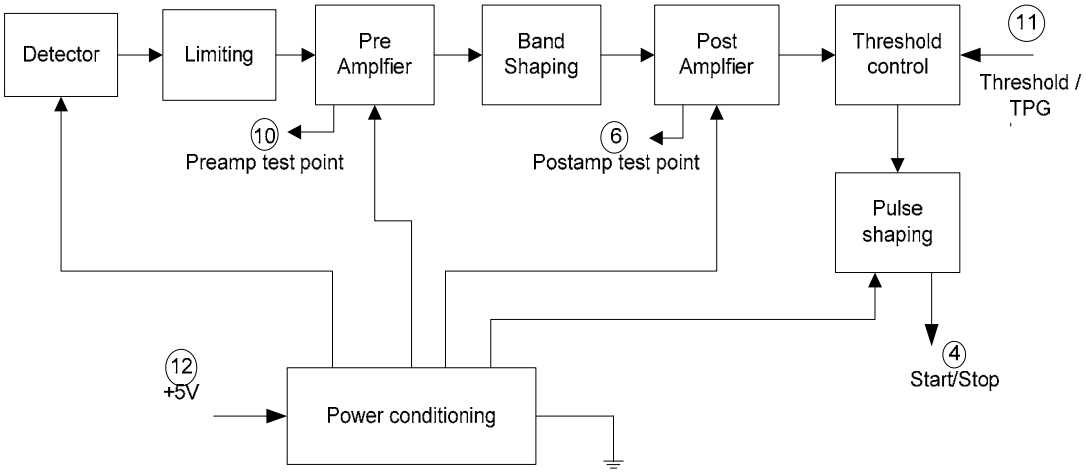

Figure 4.8 Block diagram of the electronic receiver.

4.3 Counter and Controller

The functions of the counter and controller part are: (1) to generate the sequence of timing pulse to control other boards according to the system timing diagram and (2) to convert the TOF (time-of-flight) of laser beam to range and to display the measured range.

The block diagram of the counter and controller board (CCB) is shown in Fig. 4.9. The raw start signal is generated from the integrated photodiode inside the laser head and reshaped by the signal shaper that is monostable IC 74121. The processed start pulse has 100 ns width and 3.5 V amplitude. The raw stop signal comes from the LRF receiver module and is also reshaped by a signal shaper to generate a stop pulse

that has the same property as start pulse for processing in the counter. A micro-controller is programmed to perform two functions: (1) to generate timing pulse and send the pulse to different boards in the system and (2) to count a reference clock with frequency of 25.00 MHz within the TOF duration and subsequently convert it to the measured range in the order of meter unit. The result is displayed on 4-digit matrix display. The photograph of the fabricated counter and controller board is depicted in Fig. 4.10

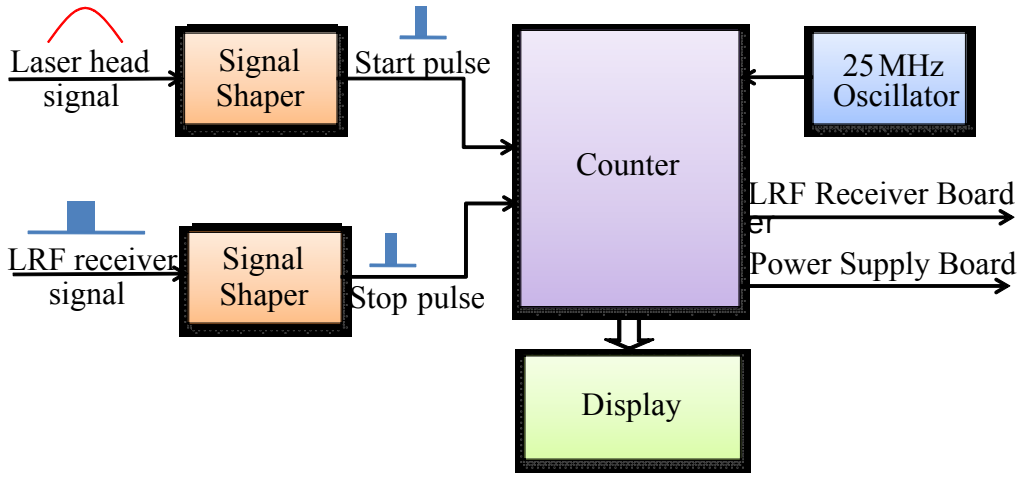

Figure 4.9 Block diagram of the counter and controller board (CCB).

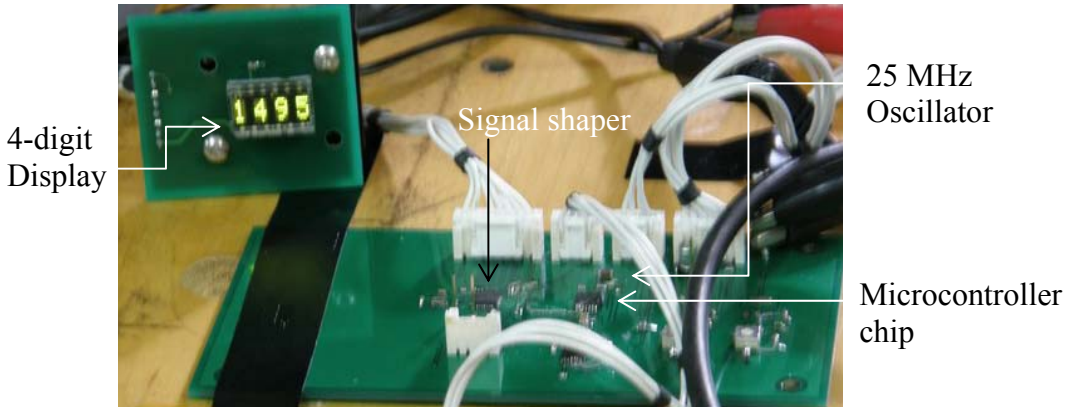

Figure 4.10 Photograph of the assembled and tested counter and controller board.

4.4 Simulation and Experimental Tests of Electronic Parts

4.4.1 Simulation Test of Counter and Controller Board

For testing the counting accuracy, we used a pulse generator (Stanford PG554) to simulate different TOFs by generating the start and the stop pulses with different time interval and feeding them to the input of CCB. After counting the number of pulses, the CCB converted the TOF into the range information. The result is shown in Table 1. The accuracy is quite good, which is 100% at range less than 1000 m, and it has small errors (+/- 5 m) for range larger than 1000 m.

Table 4.1 TOF to range conversion given by the counter and controller board.

Distance (m)	Time of Flight (ns)	Theoretical number count(hex)	Test Result (count)			Test Result (display)			Error (m)
			#1	#2	#3	#1	#2	#3	
100	670	0043	0043	0043	0043	100	100	100	0
300	2000	00CB	00C7	00C7	00C7	300	300	300	0
400	2670	010B	010C	010C	010C	400	400	400	0
500	3340	014E	014E	014E	014E	500	500	500	0
1500	10010	03E9	03EB	03EB	03EB	1505	1500	1505	+5
2000	13340	0536	0538	0535	0535	2005	2000	2000	+5
2500	16680	0648	0682	0682	0685	2495	2495	2500	-5
4000	26690	0A6D	0A6C	0A6F	0A6C	4000	4005	4000	+5
8000	53370	14D9	14DA	14DA	14DA	8000	8000	8000	0
9900	66050	19CD	19CF	19CC	19CC	9905	9900	9900	+5

4.4.2 Experimental Tests of Electronic Parts

Some experiments were performed for testing the electronic parts. The first experiment tested the power of the transmitted laser pulse which was generated when the power supply was connected to the power outlet and 10 AA batteries. In Fig. 4.11, channel 1 corresponds to the measured power due to the power outlet and

channel 2 is for 10 AA batteries. The peak amplitude of signal in channel 1 is 600 mV, while that of channel 2 is 550 mV. Therefore, the powers in channels 1 and 2 are not much different.

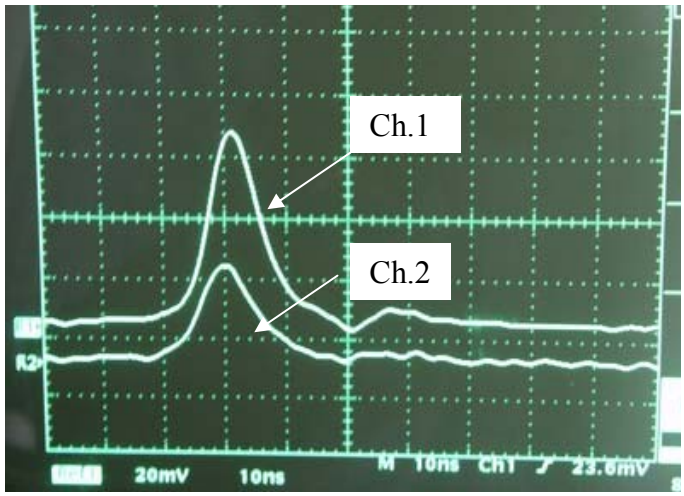

Figure 4.11 Transmitted laser power. Channel 1 is due to power outlet and channel 2 is for 10 AA batteries.

The second experiment tested the generation of the start pulse signal as shown in Fig. 4.12. In Fig. 4.12(a), channel 1 represents the original signal from the integrated photodiode inside the MK81 laser head and channel 2 represents the start pulse generated by inputting the original signal into the monostable IC 74121 of the CCB. We see that the generated start pulse happens so close to the floor level of the photodiode signal. If there is noise e.g. a surge signal from power supply, start pulse may occur earlier. Thus, it can cause false start. The signal from photodiode actually included DC bias, hence we removed the DC signal from the photodiode output using a capacitor. The resultant start pulse happens at a better position and is far from floor

level as shown in Fig. 4.12(b) where this pulse has a delay of about 51 ns from the one without DC removal.

(a)

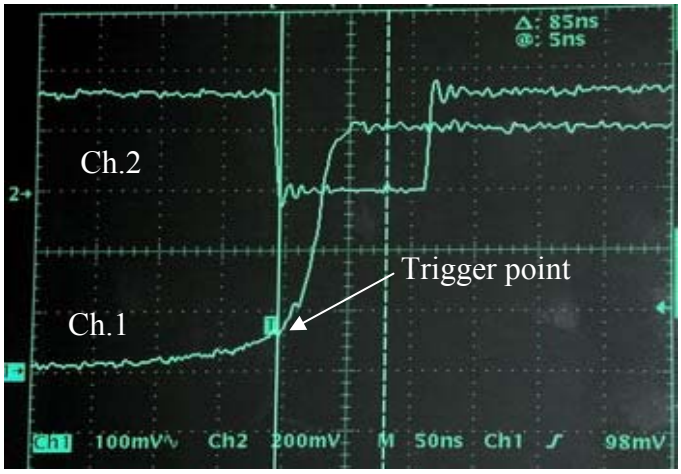

(b)

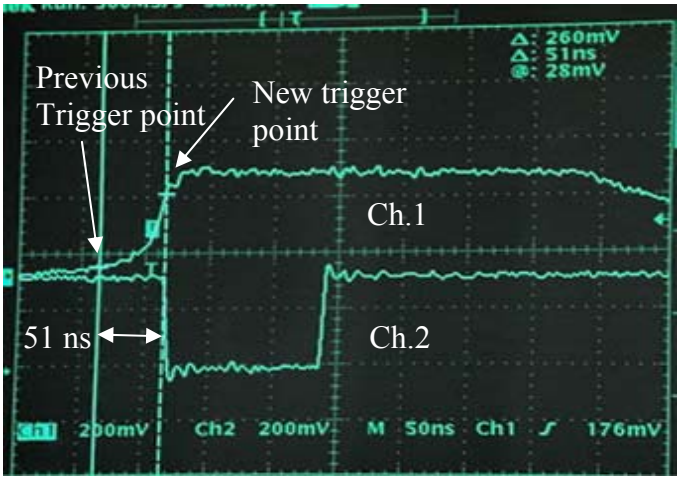

Figure 4.12 Start pulse generation. (a) Photodiode signal from laser head was fed directly to the shaper and (b) the signal was coupled by a capacitor before feeding to the shaper.

The third experiment was the receiver module test. In Fig. 4.13, channel 1 represents the signal from the preamplifier. Channel 2 shows the generated stop pulse

which is an inverted TTL with amplitude of 3.5 V and 75 ns width. In the experiment, the laser output was attenuated by a neutral density filter from 3 mJ to 29 μJ to test the minimum detectable of the receiver module. The receiver module performed consistently by producing output pulse of 3.5 V and about 100 ns pulse width. It is found that the position of the detector is very crucial such that the detector must be right at the center of the focus point in order to obtain a smooth waveform as channel 1 in Fig. 4.13.

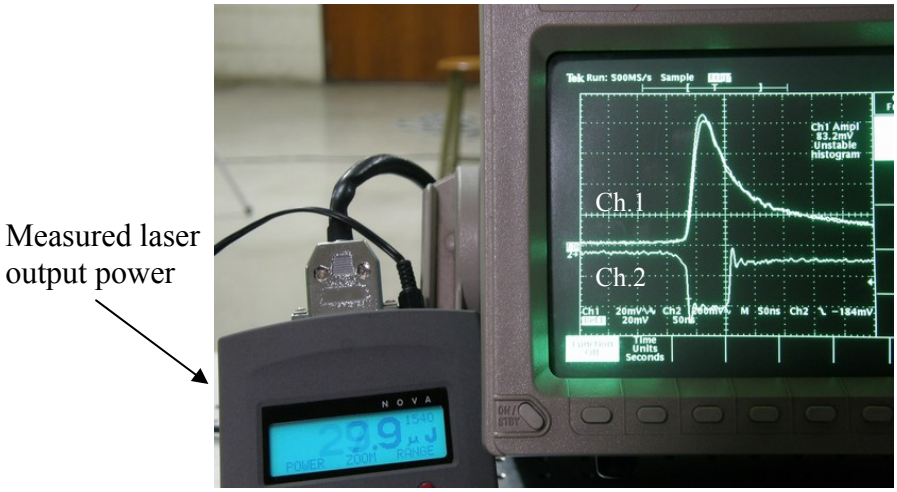

Figure 4.13 Receiver module test showing the original signal and the generated stop pulse signal.

The fourth experiment is the direct measurement of the start-stop pulse duration. The start and the stop pulses are shown in Fig. 4.14. In this experiment, the distance of measurement was 9 m and the TOF measured by the system was 85 ns. However, the calculated TOF for 9 m distance is 60 ns, thus there is a different of 25 ns which comes from the processing time different between the start and the stop

pulses. The start pulse takes less processing time than the stop pulse. This discrepancy can be corrected in the software.

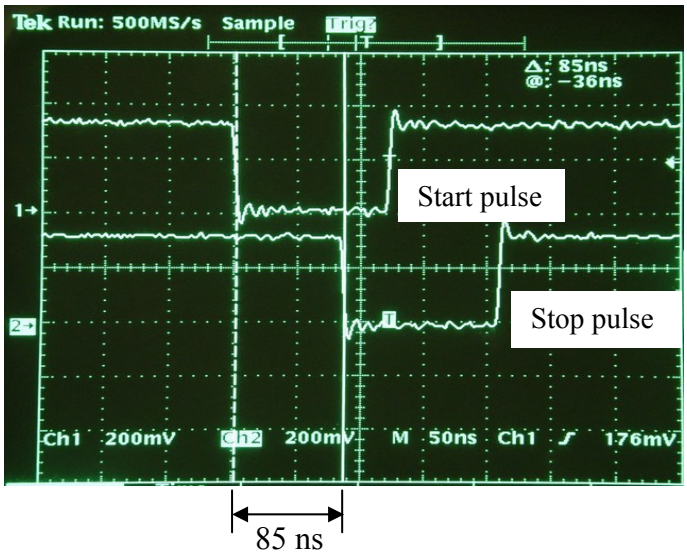

Figure 4.14 Measurement of the start-stop pulse duration.

4.5 Optical Alignment

Several experiments of optical alignment have been performed in the laboratory as follows.

4.5.1 Beam Expander Adjustment

A schematic diagram of an experimental setup for adjusting the Galilean beam expander is shown in Fig. 4.15. It is built by China Daheng Group (CDHG), China. Since the expander unit has not been calibrated, the calibration was done in our laboratory. The photograph of the setup is shown in Fig. 4.16.

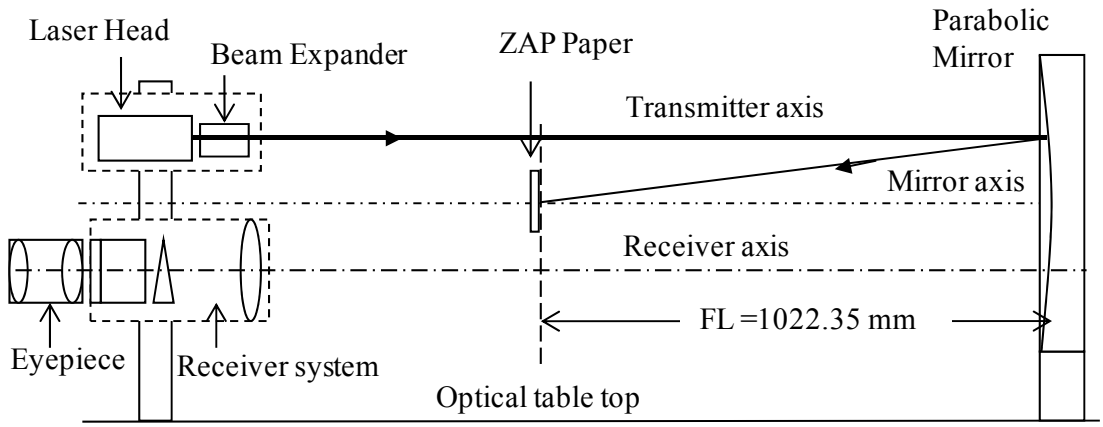

Figure 4.15 Schematic diagram of an experimental setup for beam expander adjustment.

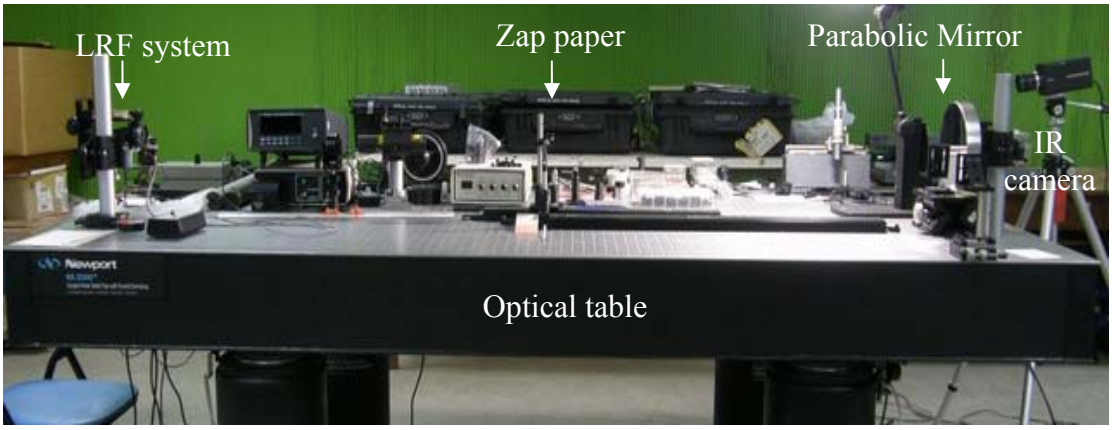

Figure 4.16 Photograph of the experimental setup of Figure 4.15.

The transmitted laser light was focused by a parabolic mirror on ZAP paper which provided thermal based estimation of the beam profile and size in real time. The paper is thermally sensitive to light over a broad spectrum from UV to IR and is useful for external alignments of optical accessories such as beam expanders, lenses, apertures, attenuators, and power measuring equipment relative to the laser beam axis. It can be simply hold or fastened in the beam path at the point where the beam imprint

is to be recorded. By pulsing the laser, a permanent visual record corresponding to the energy distribution within the laser beam is produced. Typically, the paper is used for measuring a laser pulse characterized by 1 ns to 30 ms pulse width and 5 mJ/cm² to 20 J/cm² power level.

The procedure for adjusting the beam expander was as follows. The ZAP paper was properly placed at the focal plane of the parabolic mirror with a focal length 1022.35 mm. First, the laser head fired pulses without using the beam expander toward the mirror (see Fig. 4.15). The burned pattern caused by laser spot was observed and analyzed. The burned patterns are shown in Fig. 4.17. The burned patterns from the laser alone are shown in region (a) in Fig. 4.17. The image is not sharp due to its divergence angle of 3.5 mrad that makes the spot becomes larger and power density is lower. In the second step, the beam expander was properly placed in front of the laser head. The laser was fired and the burn patterns were observed. The burned patterns are shown in region (b) in Fig. 4.17. The image is not sharp because the laser beam is not correctly collimated. In the third step, the beam expander was adjusted by adjusting the spacing between two lenses until the spot size reached the smallest. The smallest spot size indicated that the beam was collimated. The burned patterns are shown in region (c) in Fig. 4.17. The diameter of spot is 1.2 mm, hence the beam divergence is 1.2/1022.35 = 1.2 mrad. This verifies that the beam divergence is reduced by 3.5/1.2 = 3 times from the laser alone. In the fourth step, the beam expander was rotated until the focused spot superimposed with the burned pattern of the focused spot of laser alone. This indicates that the laser head and the beam expander have a common axis.

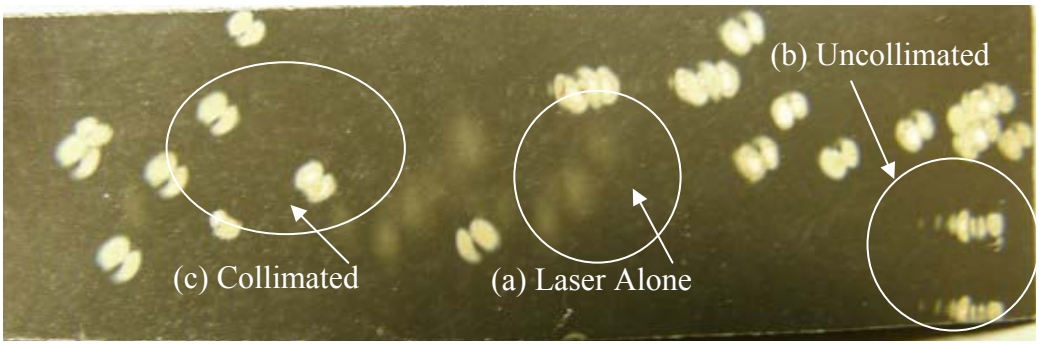

Figure 4.17 Burned patterns on ZAP paper obtained by (a) laser alone without beam expander, (b) imperfect collimated beam and (c) perfect collimated beam.

4.5.2 Bore Sighting

The bore sighting experiment is to position the target at the center of the reticle shown in Fig. 2.17 by looking through the eyepiece of the LRF. The aligning element, which is a wedge prism, is adjusted until the burned laser spot on the ZAP paper is at the center of the cross line on the reticle as shown in Fig. 4.18.

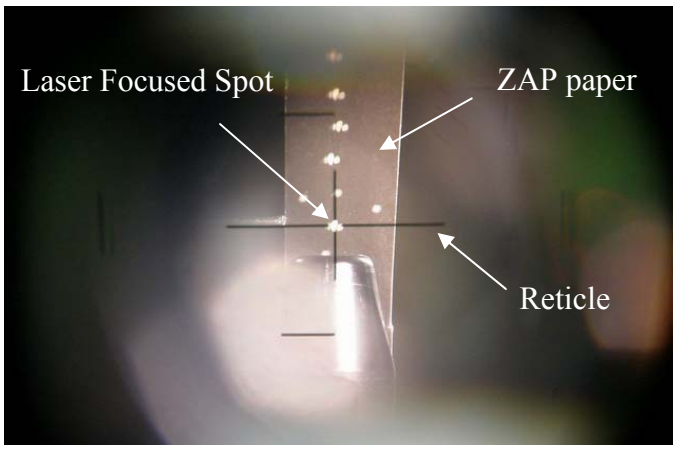

Figure 4.18 Photograph taken through the eyepiece showing bore sighting in which the laser spot is at the center of the reticle.

With this alignment, the target appearing at the cross line, which is the center of the receiver, will be also at the center of the transmitted light beam. In other words, the optical axes of the optical receiver and the transmitter are parallel.

4.6 Laser Echo Detection Experiments

Some experiments have been performed to detect the returned laser pulse or echo signal. The first experimental result is shown in Fig. 4.19 where channel 1 (lower curve) represents the start signal from the photodiode inside the laser head. The signal level is always the same, which is approximately 3 V with rise time about 9 ns, every time the laser is fired. Channel 2 (upper curve) represents the echo signal which was reflected by a paper box located at 3 m range. The signal was detected by DET10C high speed detector from Thorlabs Inc. This shows that the prism block and the objective lens are in a good alignment. The signal amplitude of the detected echo is about 1.6 V.

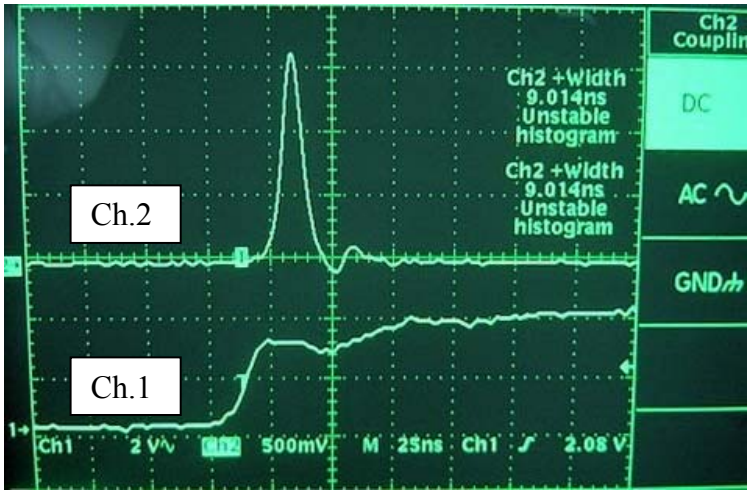

Figure 4.19 Start signal is shown in channel 1 (lower curve) and echo signal is shown in channel 2 (upper curve).

To prove that the echo signal was the signal reflected by the target instead of stray light, the objective lens which collected the echo signal was blocked for comparison. When the objective lens was blocked, there was no signal detected as shown by channel 2 (upper curve) in Fig. 4.20. Therefore, this experiment verifies that there is no stray light leaked from the transmitter unit.

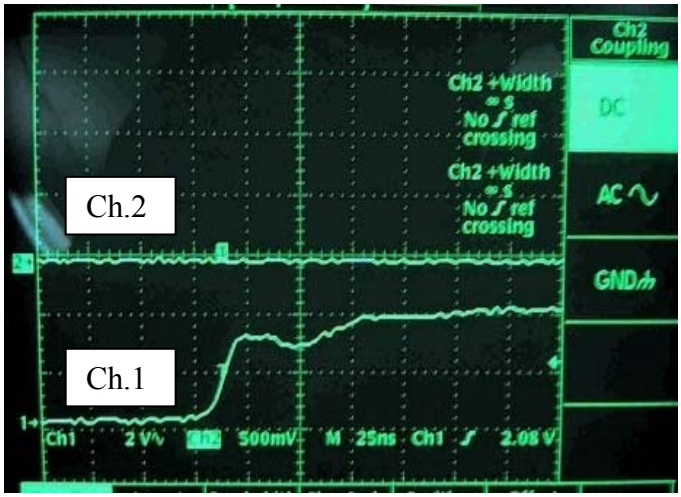

Figure 4.20 No signal is detected in channel 2 (upper curve) when the objective lens is blocked.

The second experimental result of the echo detection is shown in Fig. 4.21. In Fig. 4.21(a), channel 1 corresponds to the detected echo signal when the detector plane is not perpendicular to the objective lens axis, while Fig. 4.21(b) represents the detected signal (channel 1) when detector plane is perpendicular to the lens axis. Note that the stop pulse corresponding to channel 2 has a better shape and less noise. The ripple on the detected echo signal may come from multiple reflections of the detector window.

(a)

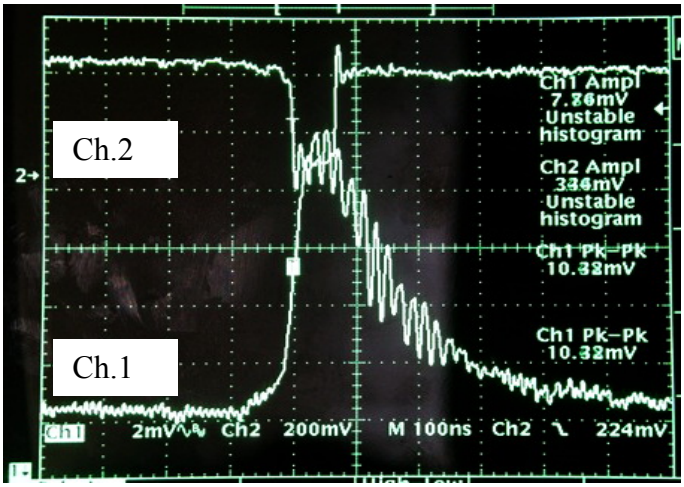

(b)

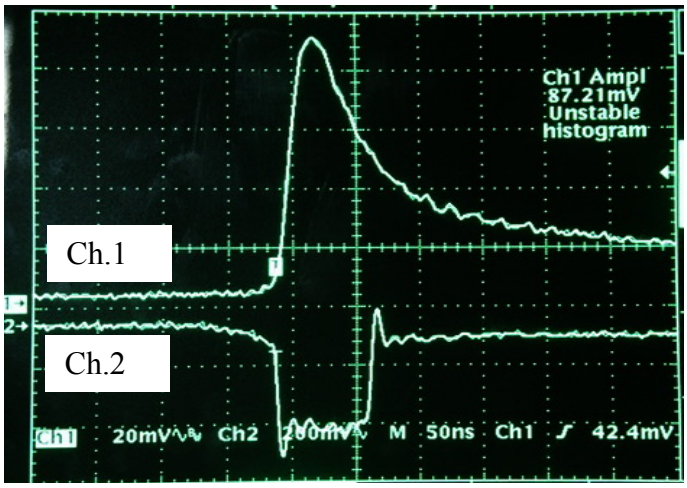

Figure 4.21 Echo signal from the receiver module. (a) The detector plane is not and (b) is perpendicular to the objective lens axis, respectively.

After completion of the testing and alignments, the eye-safe LRF was constructed as shown in Fig. 4.22. Field tests were then done by pointing the constructed LRF at a center of the tank target. Echo signals from the target located at distance up to 2000 m were successfully detected with an error of +/- 5 m. From the test data, we calculated the operational coefficient $\boldsymbol{C_{GB}}$ which was approximately

equal to 0.06. This low coefficient indicates that the constructed system performance has not been maximized. This may be caused by

- Aberration of the beam expander, i.e., beam having aberration diverges faster than the Gaussian beam.
- Imperfect collimation of the beam expander.
- Imperfection alignment of optical axis of the transmitter and the receiver systems.

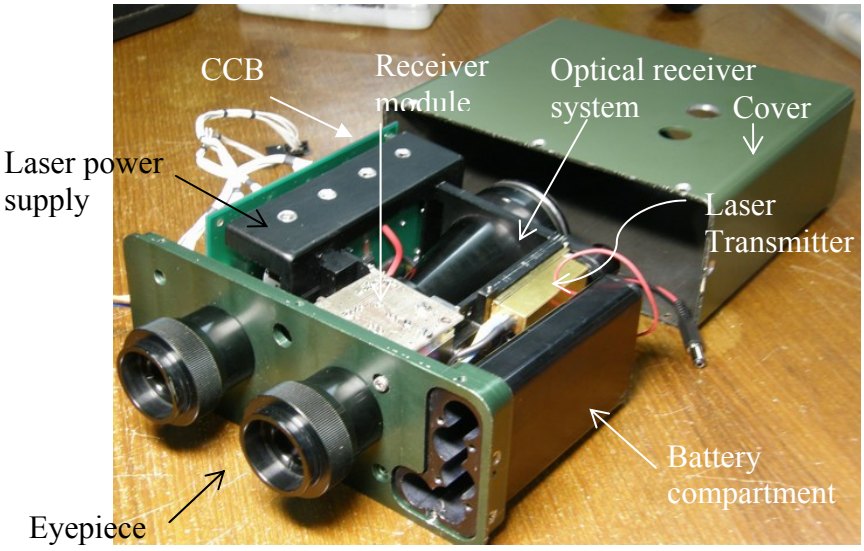

Figure 4.22 Photograph of the constructed eye-safe LRF.

4.7 Advantages of the Constructed LRF

The LRF presented in this dissertation consists of transmitter, receiver, time measuring unit, and optical system. The transmitter further consists of eye-safe laser, laser power supply, and collimator. The receiver consists of photodiode, trans-impedance type amplifier, voltage type post amplifier and a timing discriminator. The time discriminator changes the detected analog pulses to logic level pulses. The most

important property of the time discriminator is to keep the timing event at the same point. The time measurement unit is based on counting of the number of the clock pulses, like a time-to-digital converter. The optical system has two functions, one as sighting telescope and the other as laser light echo collector. A beam splitter is the crucial part to separate visible light from laser IR light.

In conventional LRFs, typically a flash-lamp pump solid state laser is employed. In our system, a diode pump Er:Glass laser is used. Besides emitting light at an eye-safe wavelength, the Er:Glass laser has several advantages over conventional flash-lamp pumped lasers in that the efficiency is higher and its life time is longer (10^7 shots instead of 10^5 shots); its power supply circuit is easy to handle, because it does not need huge storage capacitor, high voltage and triggering transformer. Since its dimension is small and its weight is light, the laser is a good candidate for the light source of the handheld LRF. Note that the EMI (electro-magnetic interference) radiation is generated in a flash-lamp pumped laser in the triggering process. Thus the benefits of using a diode pumped laser are: higher efficiency, no EMI radiation, easy power supply circuit design, higher repetitive rate, smaller size, better heat dissipation, and ruggedness suitable for military application, among others.

In a conventional laser range finder, a portion of the transmitted pulse is reflected toward the prism block. The reflected transmitted pulse enters the prism block and reaches the IR detector resulting in a start signal. In our system, a new type eye-safe laser diode pumped Er:Glass laser is employed. This laser is equipped with a built in photodetector to detect the laser light emitted from the high-reflectivity mirror. Therefore no laser light is directed to the prism block, this will significantly simplify

the optical design and alignment, and also simplify the electronic part since the start signal is already in electronic form and separated from echo signal.

CHAPTER V

CONCLUSION

5.1 Conclusion

In this dissertation, a new eye-safe LRF has been developed and verified. The experimental verifications show that the proposed LRF can measure range up to 2000 m with error +/- 5 m. The main feature of this new LRF is the use of a laser diode pumped Er:Glass laser, in contrast to a flash-lamp pumped solid state laser in conventional LRFs. The anticipated advantages of the new eye-safe LRF include:

(1) The laser emits light at 1540 nm, which is strongly absorbed by the cornea and cannot reach the retina, hence it is eye-safe.

(2) The transmitter is compact and light-weight because its lasing rod is pumped by laser diode which is compact, light-weight and free from complicated driving circuit. Furthermore, the efficiency of the laser diode pump is higher, thus the battery can last longer.

(3) Unlike conventional LRFs which generate start pulse by sampling optically the transmitted laser light, our proposed LRF has a built-in photodetector in the transmitter to detect light emitted from the back end of the laser rod (the front end emits high power pulse), thus the start signal is already in electronic form and separated from the echo signal. This will simplify construction of both optics and electronics of the new LRF.

In this study, we derive, for the first time, the new Gaussian beam range equation, and propose, also for the first time, the new concept of operational coefficient for range equations. Two widely known conventional range equations are exclusively used when (1) the target reflects totally the transmitted beam, and (2) the target reflects partially the transmitted beam. The equation for case (1) will provide erratic results if it is applied to case (2), and vice versa. By using data from our assembled eye-safe LRF, the numerical computations show that the proposed Gaussian beam range equation can be applied to both cases (1) and (2) and provide correct results.

The new operational coefficient $\boldsymbol{C_{GB}}$ is used for correcting the estimation of the maximum detectable range of LRF. First, $\boldsymbol{C_{GB}}$ is calculated from a measurement. Later, $\boldsymbol{C_{GB}}$ is used as a correcting or calibrating factor for the range equation. $\boldsymbol{C_{GB}}$ can also be used to indicate the integrated optic-electronic quality of LRF.

5.2 Future Work

The field test shows that the developed LRF still needs improvement, because the operational coefficient is quite low, less than 10%. The improvement may include: (1) alignment between transmitter and receiver, (2) optical quality of the beam expander, (3) collimation of the beam expander, (4) optical quality of the objective lens. However, it is believed that electronic parts of the system meet the expectation, because from laboratory test it is apparent that the results are satisfactory.

It is believed that this study has shown an important step in the cooperation between academia and military in research and development in Thailand. With further

improvement – mainly in optics, the made-in-Thailand laser range finders can be in production.

REFERENCES

REFERENCES

Alcock, A., DeMichelis, C. and Richardson, M. (1970). Breakdown and self-focusing effects in gases produced by means of a single-mode ruby laser. Quantum Electronics, **IEEE Journal** Vol.6, Issue 10, Oct, 622-629.

Amann, M.C, Bosch, T., Lescure, M., Myllyla, R. and Rioux, M. (2001). Laser ranging, a critical review of usual techniques for distance measurement. **Optical Engineering**, 40, 10-19.

Corcoran, V.J. (1991). High repetition rate eye-safe rangefinder. Eye-safe Lasers: Components, Systems and Applications, **Proc. SPIE** Vol. 1419, 160-169.

Einstein, A. (1917). On the quantum theory of radiation. **Physika Zeitschrift**, 18, 121-128.

Forrester, P. A. and Hulme, K. F. (1981). Laser rangefinders, **Optical and Quantum Electronics** 13, 259-293.

Franks, J.K. (1991). What is eye-safe? Eye-safe Lasers: Components, Systems and Applications, **Proc. SPIE** Vol. 1419, 2-8.

Gedcke, D.A. and McDonald, W.J. (1968). Design of the constant fraction of pulse height trigger for optimum time resolution, **Nuclear Instruments and Methods** 58, 82-84.

Hecht, E. (2002). **Optics**. Addison Wesley, San Francisco.

Kingslake, R. (1983). **Optical System Design**. Academic Press, Orlando, Florida.

Moller, K.D. (1988). **Optics**. University Science Books, Mill Valley, California.

Perger, A., Metz, J.,Tiedeke, J. and Rille, E. (1991). Eye-safe diode laser rangefinder technology. in Eye-safe Lasers: Components, Systems and Applications, **Proc. SPIE Vol. 1419**, 75-83.

Planck, M. (1901). Law of energy distribution in normal spectra. **Annalen der Physik**, 4, 553-563.

Saleh, B.E.A. and Teich, M.C. (1991). **Fundamentals of Photonics**, Wiley, New York.

Siegman, A.E. (1986). **Lasers**. University Science Books, Mill Valley, California.

Stitch, M.L. (1972). Laser range finding. **Laser Handbook**. F. T. Arecchi and E. O. Schulz-Dubois, Eds., North-Holland, Amsterdam, 1745-1804.

Strand, T. (1983). Optical three dimensional sensing, **Optical Engineering**, 24, 33-40.

Wagner, W., Ullrich, A., Melzer, T., Briese, C., and Kraus, K. (2004). From single-pulse to full-waveform airborne laser scanners: Potential and practical challenges. **International Archives of Photogrammetry and Remote Sensing**, **XXth** ISPRS Congress, Istanbul, Turkey, 12-23 July 2004, CD-ROM.

Wilson, J. and Hawkes**,** J.F.B. (1987). **Lasers Principles and Applications**. Prentice Hall, London.

Wu, R., Chen, T.L., Myers, J.D., Myers, M.J., Hardy, C.R. and Driver, J.K. (2004). Eye-safe erbium glass laser transmitter study Q-switched with cobalt spinel. Laser Radar Technology and Applications IX, **Proc. SPIE** Vol. 5412, 117-125.

CURRICULUM VITAE

Name:	Capt. Sahapong Kruapech RTN
Date of birth:	3 September 1959
Place of birth:	Prachinburi, Thailand
Nationality:	Thai
Address:	50 Ladplakao 32, Jorakaebou, Ladpraw, Bangkok 10230, Thailand.

Education

1981-1985	B.Sc. (Electrical Engineering), Naval Academy, Samutprakarn, Thailand
1986-1987	MS.EE., University of Pittsburgh, PA, USA
1998	Trainee (Laser Technology), Macquarie University, North Ryde, Australia

Awards

1995	Distinguished Researcher of Military Research and Development Center
2003	Distinguished Researcher of Defense Ministry

Publication

Kruapech S., Jutamulia S., Maitreechit S. (2004). Optical Fiber for Firing Signal Detection in Eye Safe Laser Range Finder. National Conference on Optics and Applications Processing. 67-69.